bioRxiv preprint doi: https://doi.org/10.1101/2022.06.20.496788; this version posted June 21, 2022. The copyright holder for this preprint (which was not certified by peer review) is the author/funder. All rights reserved. No reuse allowed without permission.

Retinal energy metabolism: Photoreceptors switch between Cori, Cahill, and mini-Krebs cycles to uncouple glycolysis from mitochondrial respiration

Yiyi Chen[1, 6], Laimdota Zizmare[2, 6], Victor Calbiague[3], Shirley Yu[1], Friedrich W. Herberg[4], Oliver Schmachtenberg[3], François Paquet-Durand [1, 6, 7*], Christoph Trautwein[2, 6]

[1] Institute for Ophthalmic Research, University of Tübingen, 72076, Germany
[2] Werner Siemens Imaging Center, Department of Preclinical Imaging and Radiopharmacy, University of Tübingen, 72076, Germany
[3] Centro Interdisciplinario de Neurociencia de Valparaíso, Universidad de Valparaíso, Chile
[4] Biochemistry Department, University of Kassel, 34132, Germany
[6] These authors contributed equally
[7] Lead contact
*Corresponding author: francois.paquet-durand@klinikum.uni-tuebingen.de

Summary

The retina consumes massive amounts of energy, yet its metabolism remains poorly understood. Here, we manipulated retinal energy metabolism under entirely controlled conditions and utilised ^{1}H-NMR metabolomics, *in situ* enzyme detection, and cell viability readouts to uncover the pathways of retinal energy production. Our experiments resulted in varying degrees of photoreceptor degeneration, while the inner retina and retinal pigment epithelium were essentially unaffected. Notably, rod photoreceptors relied strongly on oxidative phosphorylation, but only mildly on glycolysis. Conversely, cone photoreceptors were highly dependent on glycolysis but insensitive to electron transport chain decoupling. Moreover, photoreceptors uncouple glycolytic and Krebs-cycle metabolism via three different pathways: 1) the mini-Krebs cycle, fuelled by glutamine and branched chain amino acids, generating N-acetylaspartate; 2) the alanine-generating Cahill cycle; 3) the lactate-releasing Cori cycle. These findings forward the understanding of retinal physiology and pathology, and shed new light on neuronal energy homeostasis and the pathogenesis of neurodegenerative diseases.

bioRxiv preprint doi: https://doi.org/10.1101/2022.06.20.496788; this version posted June 21, 2022. The copyright holder for this preprint (which was not certified by peer review) is the author/funder. All rights reserved. No reuse allowed without permission.

Keywords

Energy homeostasis, tricarboxylic acid cycle, astrocyte-neuron lactate shuttle, glucose transport, N-acetylaspartate, anaplerotic substrates, aerobic glycolysis, glucose-alanine cycle, alanine transaminase, aspartate amino transferase

Abbreviations

1,9-DDF – 1,9 dideoxyforskolin, AA – amino acids, AAT – aspartate amino transferase, ADP – adenosine diphosphate, ALT – alanine transaminase, ATP – adenosine triphosphate, BCAA – branched chain amino acid, COX – cytochrome oxidase, GAC – glutaminase C, GCs – ganglion cells, GLUT - glucose transporter, GS – glutamine synthase, GTP – guanosine triphosphate, GABA – gamma amino butyric acid, GPC – sn-glycero-3-phosphate, FCCP – carbonyl cyanide-*p*-trifluoromethoxyphenylhydrazone, GSSG – glutathione disulfide, INL – inner nuclear layer, MGC – Müller glial cells, NAA – N-acetylaspartate, NAD^+ – nicotinamide adenine dinucleotide, ONL – outer nuclear layer, O-PE – O-phosphoethanolamine, OXPHOS – oxidative phosphorylation, PARP – poly(ADP)ribose polymerase, PCK – pyruvate carboxy kinase, PKM – pyruvate kinase M, PNA - peanut agglutinin, RP – retinitis pigmentosa, RPE – retinal pigment epithelium, RPE65 – retinal pigment epithelium-specific 65 kDa protein, SUCLG1 – succinate-CoA ligase-1, TUNEL – terminal UDP nick-end labelling, UDP – uracil diphosphate

bioRxiv preprint doi: https://doi.org/10.1101/2022.06.20.496788; this version posted June 21, 2022. The copyright holder for this preprint (which was not certified by peer review) is the author/funder. All rights reserved. No reuse allowed without permission.

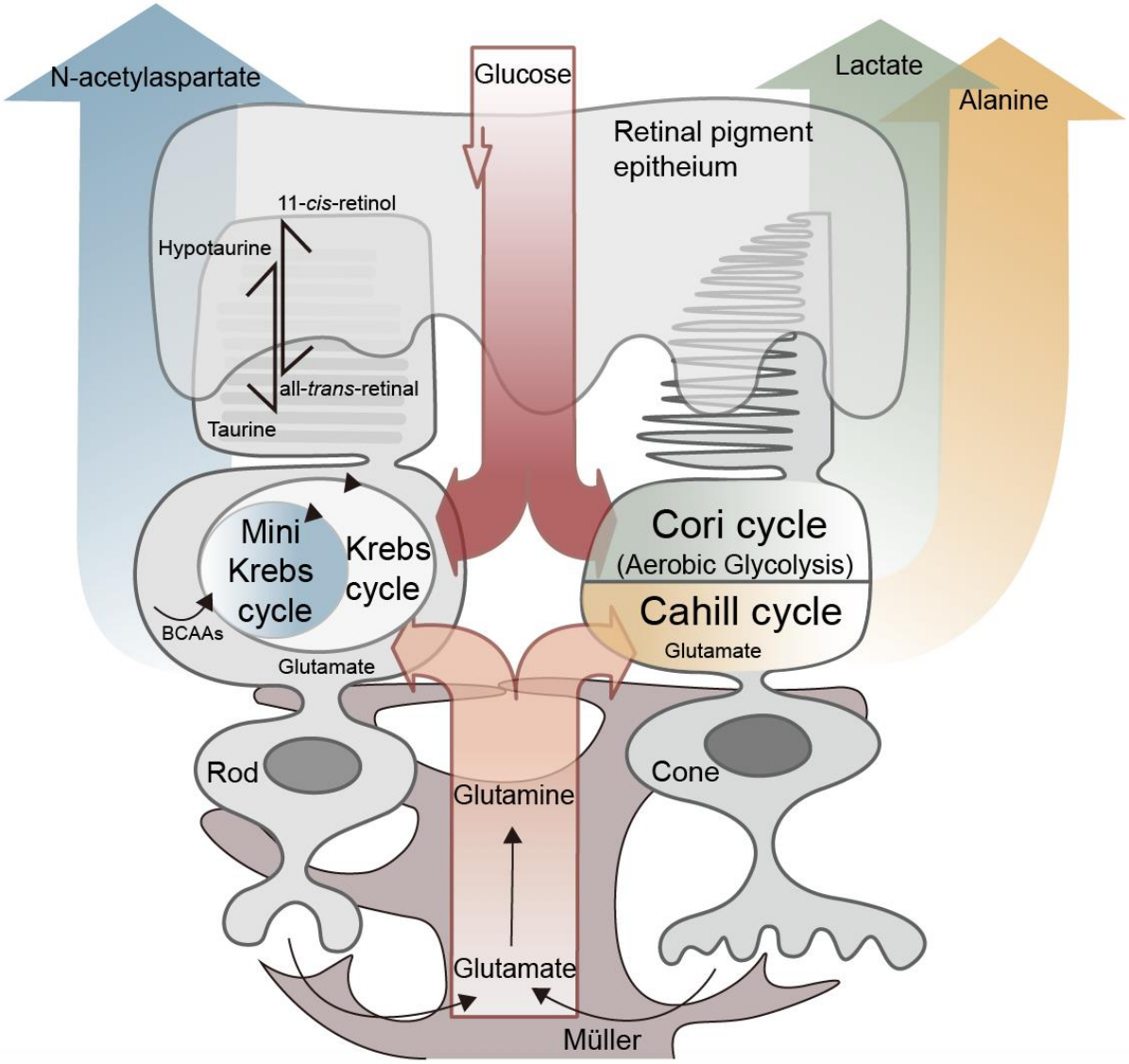

Graphical abstract: Retinal photoreceptors employ both glucose and anaplerotic substrates as fuels. While rod photoreceptors rely strongly on oxidative phosporylation and the N-acetylaspartate producing mini Krebs-cycle, cone photoreceptors rely much more on the lacate-producing Cori-cycle and the oxidative, alanine-producing Cahill-cycle.

bioRxiv preprint doi: https://doi.org/10.1101/2022.06.20.496788; this version posted June 21, 2022. The copyright holder for this preprint (which was not certified by peer review) is the author/funder. All rights reserved. No reuse allowed without permission.

Introduction

The retina is the neuronal tissue with the highest energy demand[1,2]. Paradoxically, the mammalian retina has been suggested to strongly rely on energy-inefficient glycolysis, even though oxygen and high energy yield oxidative phosphorylation (OXPHOS) would be available[3]. This aerobic glycolysis releases large amounts of lactate, as already reported in the 1920s by Otto Warburg[4]. High retinal energy demand is linked to the extraordinary single-photon sensitivity of photoreceptors[2,5,6], as well as to lipid synthesis for the constant renewal of photoreceptor outer segments[7,8].

The retina harbours two types of photoreceptors: rods, which exhibit remarkable light sensitivity and enable night vision; and cones, which work in daylight and allow colour vision. Cones spend around twice as much energy as rods[9]. Photoreceptors are not connected to the vasculature and are nourished by other retinal cell types, including retinal pigment epithelial (RPE) cells or Müller glial cells (MGC). Moreover, photoreceptors can experience changes in energy demand on a millisecond timescale, from very high in the dark, to much lower in light.

Glycolysis provides for rapid but inefficient ATP production, while Krebs cycle and OXPHOS are very efficient but much slower. Since glycolysis and Krebs cycle are metabolically coupled through pyruvate, it is unclear how photoreceptors adapt to sudden and large changes in energy demand. Also, what energy substrates and shuttles are used by photoreceptors, is a matter of debate[10,11]. A recent hypothesis proposed that photoreceptors use predominantly aerobic glycolysis, with the resultant lactate utilized by the RPE and MGCs for OXPHOS[10,12]. However, this is in contrast with the high density of mitochondria in photoreceptor inner segments. Retinal energy metabolism has obvious ramifications for the pathogenesis of diseases, including diabetic retinopathy, age-related macular degeneration, or inherited retinal diseases, such as retinitis pigmentosa.

Here, we studied expression of energy metabolism-related enzymes in different retinal cell types, using organotypic retinal explants maintained in serum-free, fully defined medium. Metabolic functions of the RPE were investigated by culturing retina with and without RPE. As readouts, we correlated

bioRxiv preprint doi: https://doi.org/10.1101/2022.06.20.496788; this version posted June 21, 2022. The copyright holder for this preprint (which was not certified by peer review) is the author/funder. All rights reserved. No reuse allowed without permission.

enzyme expression with proton nuclear magnetic resonance (^{1}H-NMR) spectroscopy-based metabolomics and cell death. Notably, interventions in energy metabolism caused selective photoreceptor cell death, while leaving other retinal cell types unaffected. Metabolomic analysis and localization of key enzymes identified novel pathways and shuttles, explaining the strong interdependence of the various retinal cell types, and opening new perspectives for the treatment of neurodegenerative diseases in the retina and beyond.

Results

Retinal expression patterns of key energy metabolism related enzymes

We used immunofluorescence to assess expression and cellular localization of enzymes important for retinal metabolism (Figure 1). The outermost retinal layer is formed by RPE cells expressing RPE-specific 65 kDa protein (RPE65), dedicated to the recycling of photopigment retinal[13]. Hence, immunolabeling for RPE65 revealed the RPE cell monolayer (Figure 1A). Immunofluorescence for glucose-transporter-1 (GLUT1) showed a strong labelling on both basal and apical sides of RPE cells (Figure 1A), in line with previous literature[14-16]. Glucose uptake from the RPE into the neuroretina is mediated by high affinity/high capacity GLUT3[17] strongly expressed on photoreceptor inner segments (Supplementary Figure 1). Pyruvate kinase is essential to glycolysis, catalyzing the conversion of phosphoenolpyruvate to pyruvate. While pyruvate kinase M1 (PKM1) was expressed in the inner retina (Supplementary Figure 1), PKM2 was located to the outer nuclear layer (ONL), in photoreceptor inner segments and synapses (Figure 1A). Expression of mitochondrial cytochrome oxidase (COX) largely overlapped with PKM2 (Figure 1A).

bioRxiv preprint doi: https://doi.org/10.1101/2022.06.20.496788; this version posted June 21, 2022. The copyright holder for this preprint (which was not certified by peer review) is the author/funder. All rights reserved. No reuse allowed without permission.

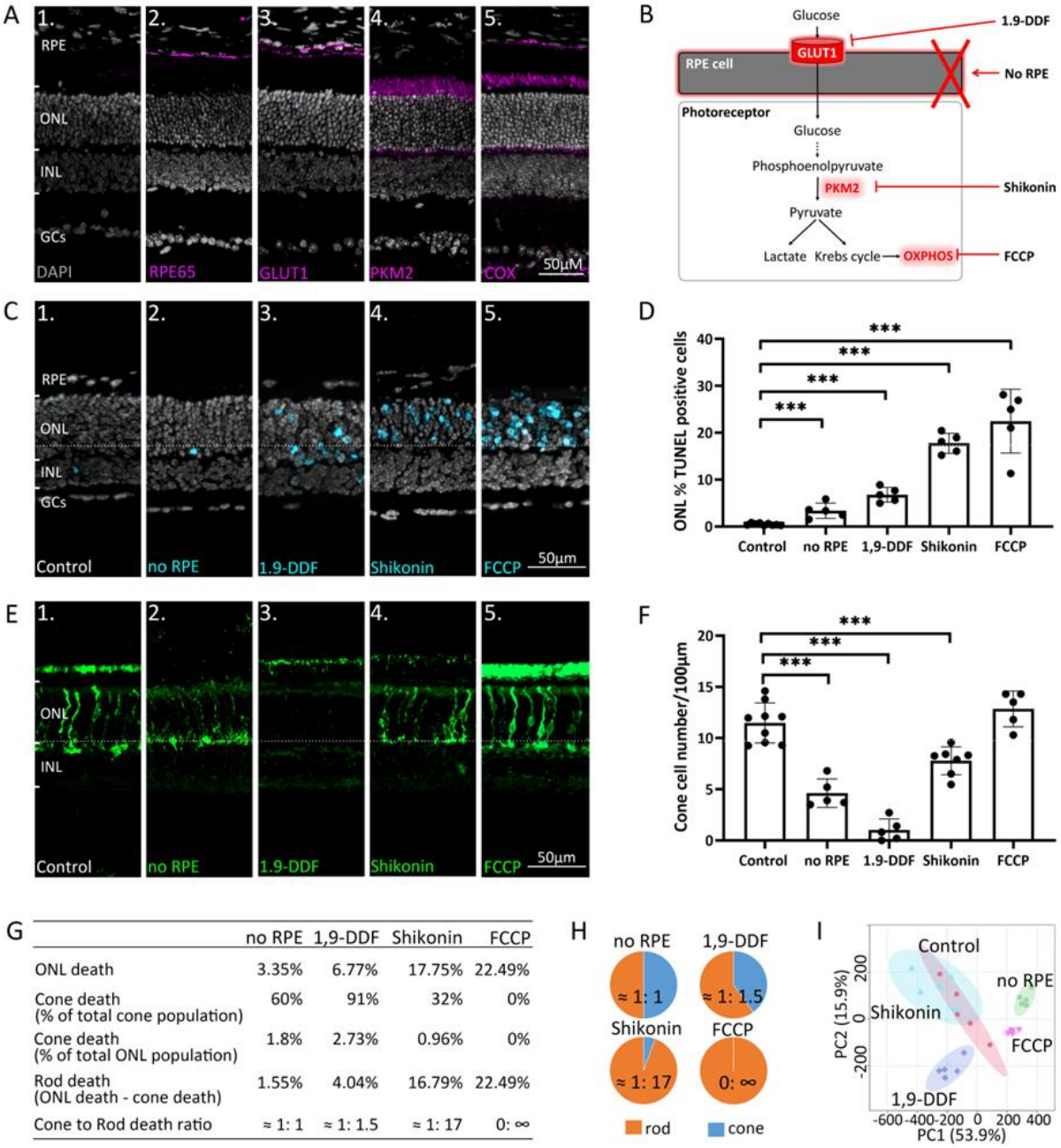

	no RPE	1,9-DDF	Shikonin	FCCP
ONL death	3.35%	6.77%	17.75%	22.49%
Cone death (% of total cone population)	60%	91%	32%	0%
Cone death (% of total ONL population)	1.8%	2.73%	0.96%	0%
Rod death (ONL death - cone death)	1.55%	4.04%	16.79%	22.49%
Cone to Rod death ratio	≈ 1: 1	≈ 1: 1.5	≈ 1: 17	0: ∞

Figure 1. Manipulating energy metabolism differentially affects rod and cone photoreceptors. (**A**) Immunofluorescence staining (magenta): (A1) negative control, (A2) RPE65, (A3) glucose transporter-1 (GLUT1), (A4) pyruvate kinase M2 (PKM2), (A5) mitochondrial cytochrome oxidase (COX). (**B**) Overview of experimental manipulations. Organotypic retinal explants were cultured with or without RPE or treated with 1,9-DDF, Shikonin, or FCCP. (**C**) TUNEL assay (cyan) marking dying cells in the five experimental conditions. (**D**) Quantification of TUNEL-positive cells in outer nuclear layer (ONL). Data represented as mean ± SD. (**E**) Cone-arrestin labelling (green) in the ONL. (**F**) Quantification of arrestin-positive cones. Data represented as mean ± SD. (**G**) Table giving percentages of cones and rods lost for each treatment. (**H**) Pie charts illustrate cone to rod cell death ratios. (**I**) Principal component analysis (PCA) of retinal samples investigated with ^{1}H NMR spectroscopy-based metabolomics. Dots in graphs represent individual retinal explants. Asterisks indicate significance levels: *p<0.05, **p<0.01, *** p<0.001. RPE = Retinal pigment epithelium; INL = inner nuclear layer; GCs = ganglion cells.

bioRxiv preprint doi: https://doi.org/10.1101/2022.06.20.496788; this version posted June 21, 2022. The copyright holder for this preprint (which was not certified by peer review) is the author/funder. All rights reserved. No reuse allowed without permission.

Challenging energy metabolism reduces rod and cone photoreceptor viability

To dissect retinal energy metabolism, we selectively manipulated key pathways (Figure 1B) using organotypic retinal explants[18]. Retinal cultures were prepared with the RPE cell layer attached to the neuroretina (***control***) or without RPE (***no RPE***). In ***control***, the rate of ONL cell death, as assessed by the TUNEL assay (Figure 1C, D), was low (0.46%±0.22, n=9). The ***noRPE*** condition displayed significantly increased photoreceptor cell death (3.35%±1.62, n=5, p<0.001). Blocking RPE glucose transport with the selective GLUT1 inhibitor 1,9 dideoxyforskolin (***1,9-DDF***)[19] further increased ONL cell death (6.77%±1.57, n=5, p<0.0001). The inhibition of glycolytic PKM2 with ***Shikonin***[20,21], and OXPHOS disruption with the electron chain uncoupler carbonyl cyanide-*p*-trifluoromethoxyphenylhydrazone (***FCCP***)[22] both caused a significant increase in photoreceptor cell death (***Shikonin***: 17.75%±2.13, n=5, p<0.0001; ***FCCP***: 22.49%±6.79, n=5, p<0.0001). All four experimental interventions mostly affected photoreceptors, not significantly reducing the viability of other retinal cell types (Figure 1C).

Remarkably, a differential effect on cone photoreceptor survival (Figure 1E, F) was observed as assessed by immunodetection of the cone-specific marker arrestin-3 (Arr3). ***Control*** retina harboured 11.47 (±1.95, n=9) cones per 100 µm of retinal circumference. ***noRPE*** retina displayed a significant decrease in cone survival (4.62±1.39, n=5, p<0.0001), while blocking RPE glucose transport with ***1,9-DDF*** led to an even more dramatic reduction (1.02±1.09, n=5, p<0.0001). By comparison, inhibition of glycolysis with ***Shikonin*** had a relatively mild effect on cone survival (7.78±1.36, n=5, p<0.0001). Surprisingly, ***FCCP*** treatment did not cause cone death (12.84±1.75, n=5, p=0.22), compared to ***control***.

We further calculated the percentages of dying cones and rods, assuming that 3% of all photoreceptors were cones[23,24] (Figure 1G, H). In the four treatment situations the ratios of cone to rod death were: ***no RPE*** = 1:1; ***1,9-DDF*** = 1:1.5; ***Shikonin*** = 1:17; and ***FCCP*** = 0: ∞. Cones were almost entirely depleted by the ***1,9-DDF*** treatment but remained virtually unaffected by the ***FCCP*** treatment. Rods, however, were strongly and highly selectively affected by ***Shikonin*** and ***FCCP***, while the ***no RPE*** condition had a

bioRxiv preprint doi: https://doi.org/10.1101/2022.06.20.496788; this version posted June 21, 2022. The copyright holder for this preprint (which was not certified by peer review) is the author/funder. All rights reserved. No reuse allowed without permission.

relatively minor effect. These results highlight important differences between rod and cone energy metabolism.

Experimental retinal interventions produce characteristic metabolomic patterns

We employed high-field (600 MHz) ^{1}H-NMR spectroscopy-based metabolomics to study the metabolic signatures in five experimental groups. A principal component analysis (PCA) showed clear group separation (Figure 1I). Unbiased clustering of metabolite profiles revealed specific groups that were differentiated among the five experimental situations (Figure 2A). The greatest cluster overlap was seen in ***control*** and ***Shikonin*** groups. Significant clustering was observed in several amino acid sub-classes and energy metabolites. We found the strongest changes in the ***1,9-DDF*** condition, where glutamate, aspartate, alanine, O-phosphocholine, and nicotinamide adenine dinucleotide (NAD^{+}) concentrations were particularly upregulated compared to control. Further, branched-chain amino acids (BCAAs), lactate, and threonine were upregulated in the ***FCCP*** and ***no RPE*** condition. Glutathione (GSH) and glutathione disulfide (GSSG) were relatively reduced by ***Shikonin***, which increased creatine and formate. ***Control*** and ***1,9-DDF*** treatment displayed high levels of guanosine triphosphate (GTP), adenosine triphosphate (ATP), and π-methylhistidine, which were low in the other groups (Figure 2A).

We then compared metabolite patterns for each treatment to ***control*** (Figure 2B). Metabolites were grouped according to class and function, including fundamental metabolic pathways, such as energy and cofactor metabolism, coenzymes, Krebs cycle, neuronal tissue-associated metabolites and neurotransmitters, BCAAs, glucogenic and ketogenic amino acids (AAs), serine synthesis pathway, cell membrane synthesis (Kennedy pathway), and individual features from redox metabolism. Afterwards, the metabolomic differences identified were explored in detail and related to the retinal expression of corresponding enzymes.

bioRxiv preprint doi: https://doi.org/10.1101/2022.06.20.496788; this version posted June 21, 2022. The copyright holder for this preprint (which was not certified by peer review) is the author/funder. All rights reserved. No reuse allowed without permission.

A

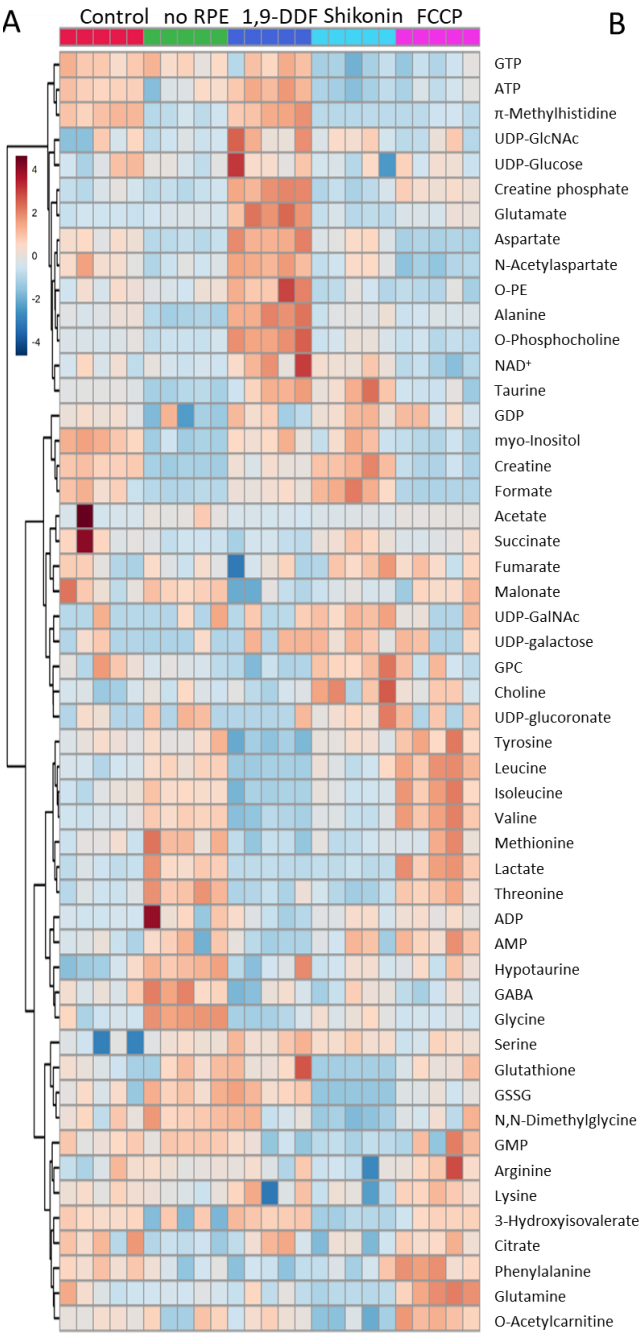

B

Class	Function	Metabolite	no RPE		1,9-DDF		Shikonin		FCCP	
			p	FC	p	FC	p	FC	p	FC
Nucleotides	Energy metabolism, cofactors	**ATP**	↓*	0.8	↑**	1.1	↓****	0.6	↓***	0.7
		ADP					↑*	1.3	↑***	1.5
		AMP							↑**	1.8
		GTP					↓****	0.6	↓***	0.7
		GDP								
		GMP					↓***	0.4		
	Coenzyme	**NAD+**			↑*	1.3			↓*	0.8
		UDP-GalNAc					↑*	3.2		
		UDP-GlcNAc			↑*	1.5				
Organic Acids	Glycolysis	**Lactate**	↑***	3.7					↑***	4.6
	Krebs cycle	**Citrate**	↓*	0.7						
		Fumarate								
		Succinate								
	Mitochondria	**Formate**	↓**	0.2					↓**	0.2
	Osmolyte	**Taurine**	↓****	0.9	↑*	1.1	↑*	1.1		
		Hypotaurine	↑***	1.9						
	Neuronal tissue-associated metabolite	**GABA**	↑**	1.1						
		Malonate			↓*	0.4				
		NAA	↓*	0.8	↑*	1.2			↓***	0.6
		Creatine	↓****	0.6	↓***	0.9			↓***	0.6
		Creatine phosphate			↑****	1.6			↑**	
Amino Acids	Neuro-transmitter, Krebs cycle	**Glutamate**	↑**	1.1	↑****	2.1			↑**	1.2
	BCAA	**Isoleucine**	↑**	1.3	↓**	0.7			↑**	1.6
		Leucine	↑***	1.3	↓***	0.8			↑***	1.5
		Valine	↑****	1.3	↓**	0.8			↑***	1.5
	Glucogenic, ketogenic amino acid	**Glutamine**					↓*	0.7	↑*	1.5
		Tyrosine			↓****	0.7			↑*	1.2
		Lysine							↑*	1.1
		Phenylalanine	↓*	0.9	↓***	0.8	↓*	0.9		
		Aspartate	↓****	0.6	↑***	1.6			↓***	0.4
		Alanine	↓****	0.8	↑****	1.5			↓**	0.9
	Serine synthesis pathway, one carbon metabolism	**Methionine**	↑**	2.1	↓*	0.4				
		Serine	↑*	1.7	↑*	2.0	↑*	1.8		
		Glycine	↑****	1.6						
		Threonine	↑****	1.4					↑***	1.3
		π-Methyl-histidine	↓****	0.2			↓****	0.1	↓***	0.2
		N,N-Dimethyl-glycine	↑*	1.2			↓***	0.6		
Lipids and growth	β-oxidation of fatty acids	**O-Acetyl-carnitine**					↓**	0.5	↑**	1.4
		3-Hydroxy-isovalerate			↑*	1.1	↓****	0.5		
	Cell membrane synthesis, Kennedy pathway	**myo-Inositol**	↓****	0.6					↓***	0.6
		Choline					↑*	1.7	↑*	1.3
		O-Pospho-choline	↓**	0.8	↑****	2.0			↓**	0.8
		GPC			↓*	0.8				
		O-PE			↑**	1.3	↓*	0.9	↓*	0.9
Tri-peptide	Redox metabolism	**Glutathione**					↓**	0.1		
		GSSG	↑*	1.8	↑*	1.8	↓**	0.1		

Figure 2. ^{1}H-NMR spectroscopy-based metabolomic analysis of retina subjected to interventions in energy metabolism. (**A**) Heatmap (red – high, blue – low), based on unsupervised hierarchical cluster analysis by Ward's linkage, showing metabolite concentrations in five different experimental conditions: control - red, no RPE - green, 1,9-DDF - dark blue, Shikonin - light blue, FCCP purple (n = 5 samples per condition). (**B**) Metabolic profiles of each intervention were compared to control. Metabolites significantly changed in at least one experimental condition, were grouped according to functions and pathways. Data show *p*-values and fold change (FC) over control. Statistical comparison: student´s unpaired *t*-test (group variance equal); *p* values: **** < 0.0001, *** < 0.001, ** < 0.01 * < 0.05. See also Supplementary Figure 2.

bioRxiv preprint doi: https://doi.org/10.1101/2022.06.20.496788; this version posted June 21, 2022. The copyright holder for this preprint (which was not certified by peer review) is the author/funder. All rights reserved. No reuse allowed without permission.

Retina cultured without RPE displays strongly increased glycolytic activity

The RPE is tightly bound to the choroid and serves as interface between vasculature and neuroretina. Because of the strong adherence of RPE to the choroid, most prior studies on explanted retina were performed without RPE[3,4,10]. To understand the metabolic communication between neuroretina and RPE, we prepared organotypic retinal explants both with RPE (***control***) or without RPE (***no RPE***).

The metabolite profile of ***control*** was markedly different from retina cultured without RPE, with 25 metabolites exhibiting significant changes (Figure 3A, Supplementary Figure 3). Decreased ATP levels in the ***no RPE*** group, corresponded to increased lactate. The BCAAs isoleucine, leucine, and valine, and some of the glucogenic/ketogenic AAs threonine, methionine, glycine, displayed higher levels in the ***no RPE*** group compared to control. Alanine, aspartate, and taurine showed the opposite trend. Hypotaurine, 4-aminobutyrate (GABA), and glutamate displayed strong retinal accumulation, while membrane synthesis associated metabolites, such as myo-inositol and O-phosphocholine, as well as creatine and N-acetylaspartate (NAA) were reduced in neuroretina. Moreover, higher levels of GSSG appeared in the absence of RPE, pointing towards an altered redox metabolism.

Pattern hunter correlation analysis found citrate, a central Krebs cycle metabolite, positively correlated with taurine, alanine, aspartate, and ATP (Figure 3B). Negative correlations to citrate included ADP, BCAAs, and lactate. A subsequent KEGG-based pathway analysis revealed changes in arginine and proline metabolism, taurine and hypotaurine metabolism, and alanine, aspartate, and glutamate metabolism in the ***no RPE*** situation (Figure 3C).

bioRxiv preprint doi: https://doi.org/10.1101/2022.06.20.496788; this version posted June 21, 2022. The copyright holder for this preprint (which was not certified by peer review) is the author/funder. All rights reserved. No reuse allowed without permission.

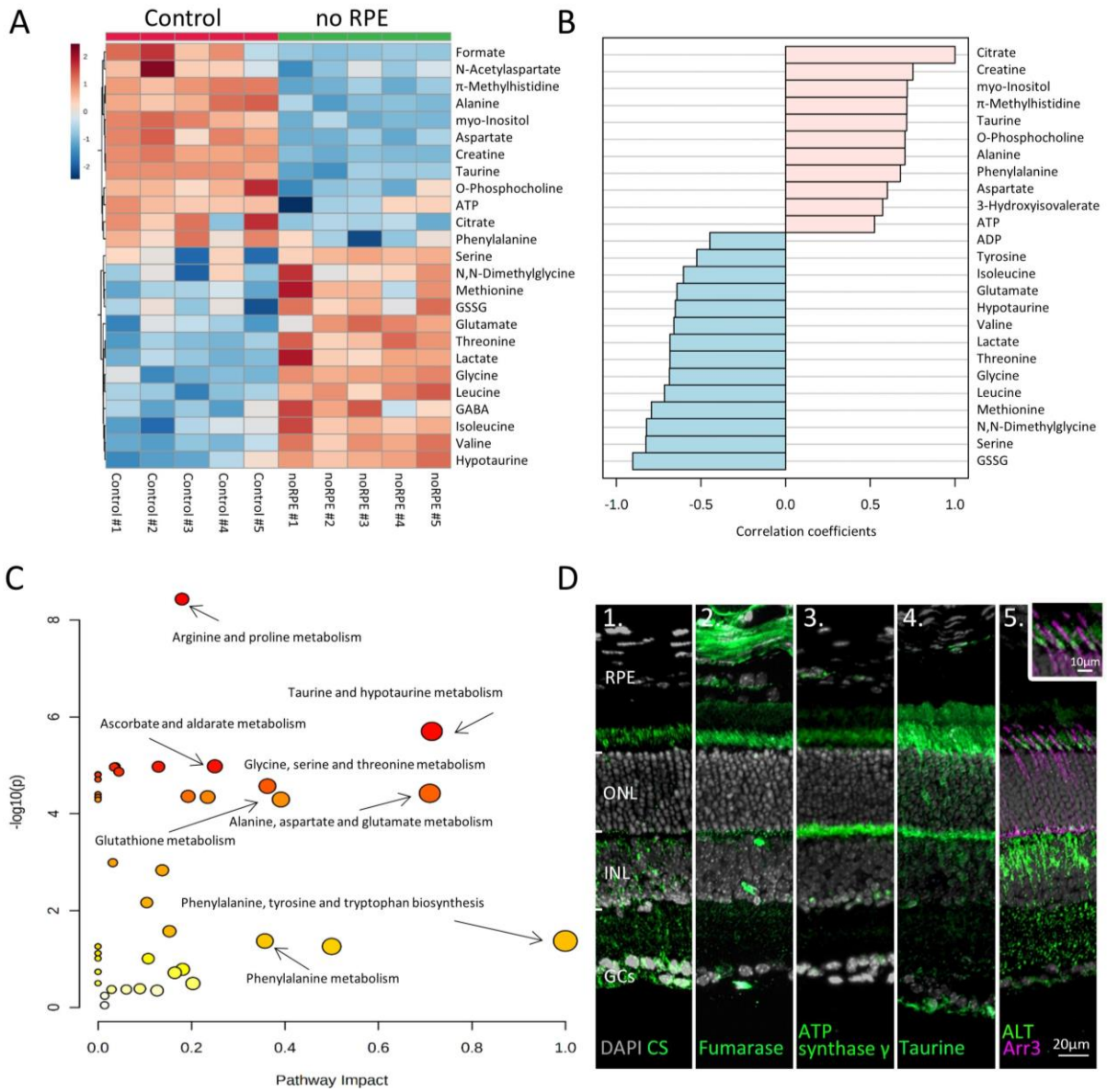

Figure 3: Absence of RPE dramatically changes retinal metabolism. (**A**) Heatmap, based on unsupervised hierarchical cluster analysis by Ward's linkage, illustrating statistically significant changes for 25 metabolites (unpaired t-test, fold change (FC) > 1.2, raw *p* value < 0.05). (**B**) Pattern hunter for citrate, showing the top 25 correlating metabolites, correlation coefficient given as Pearson r distance. (**C**) Most affected metabolic pathways by ***no RPE*** condition compared to control, based on KEGG-pathway database. (**D**) Immunodetection of enzymes and metabolites (green): (**D**1) citrate synthase (CS), (**D**2) fumarase, (**D**3), ATP synthase γ, (**D**4) taurine, (**D**5) alanine transaminase (ALT). Co-staining for ALT and cone arrestin (Arr3; magenta) showed high expression in cone inner segments. DAPI (grey) was used as a nuclear counterstain. See also Supplementary Figure 3.

Immunofluorescence was used to localize enzymes likely responsible for the observed metabolic changes (Figure 3D). Citrate synthase (CS), the key enzyme of the Krebs cycle, was found mostly in photoreceptor inner segments and synaptic terminals. The γ-subunit of ATP synthase, essential for OXPHOS, was also localized to photoreceptor inner segments and synapses. Thus, low ATP levels in the

bioRxiv preprint doi: https://doi.org/10.1101/2022.06.20.496788; this version posted June 21, 2022. The copyright holder for this preprint (which was not certified by peer review) is the author/funder. All rights reserved. No reuse allowed without permission.

no RPE group likely resulted from decreased photoreceptor Krebs cycle and OXPHOS activity. High levels of taurine were detected in photoreceptor inner segments and synapses, as well as in the ganglion cell layer (Figure 3D). Finally, the enzyme alanine transaminase (ALT), previously thought to be expressed only in muscle and liver, was found to be expressed in the inner nuclear and plexiform layers (Figure 3D). ALT was also strongly expressed in cone inner segments, as evidenced by co-labelling with cone arrestin-3 (Arr3). This expression pattern and high alanine levels in the ***control*** suggested Cahill cycle activity in the retina[25].

The patterns observed in the ***no RPE*** to ***control*** comparison indicated that retinal metabolism strongly depends on RPE-to-neuroretina interactions, including shuttling of metabolites such as hypotaurine/taurine. Notably, the accumulation of BCAA, glutamate, and lactate, concomitant with decreased alanine levels in the ***no RPE*** group, implied that RPE removal switched retinal metabolism from Krebs cycle/OXPHOS to aerobic glycolysis.

Photoreceptors use the Krebs cycle to produce GTP

We further compared metabolite patterns between ***no RPE*** and ***FCCP*** groups. In Figure 2, the ***no RPE*** and ***FCCP*** groups showed similar metabolite patterns and pathway changes overall. However, a detailed statistical analysis revealed 17 significant metabolite changes (Figure 4A; Supplementary Figure 4). Among the most highly downregulated metabolites in the FCCP group was GTP, which positively correlated with GABA, ATP, GSSG, hypotaurine, and NAD^+ (Figure 4B). In contrast, GDP, BCAAs, glutamine, and citrate negatively correlated to GTP. The KEGG-based pathway analysis ranked glycine, serine and threonine metabolism, glutathione metabolism, and alanine, aspartate and glutamate metabolism as the most significantly changed between the two conditions (Figure 4C).

The depletion of GTP in the ***FCCP*** but not in the ***no RPE*** situation raised an important question: Measurable amounts of GTP can only be generated in two ways: 1) by succinate-CoA ligase, GTP-forming-1 (SUCLG-1) in the Krebs cycle, and 2) by nucleoside-diphosphate kinase (NDK) from excess

bioRxiv preprint doi: https://doi.org/10.1101/2022.06.20.496788; this version posted June 21, 2022. The copyright holder for this preprint (which was not certified by peer review) is the author/funder. All rights reserved. No reuse allowed without permission.

ATP. Since ATP levels were low in both experimental groups, GTP could not have been produced from ATP. Immunofluorescence for SUCLG-1 showed strong expression in photoreceptor inner segments and synapses, where it co-localized to a large extent with mitochondrial COX (Figure 4D). Hence, the SUCLG-1 retinal expression pattern and the synthesis of GTP in the absence of RPE provided further evidence for Krebs cycle activity in photoreceptors.

We also identified an ***FCCP***-induced upregulation of citrate, concomitant with a downregulation of NAD^+. This indicated a Krebs cycle interruption at the level of D-isocitrate to α-ketoglutarate conversion, *i.e.*, a step that requires NAD^+. NAD^+ is known to be consumed by poly-ADP-ribose-polymerase (PARP), which is activated by oxidative DNA damage[26] and up-regulated in dying photoreceptors[27]. Therefore, we quantified poly-ADP-ribose (PAR) accumulation in retinal cells as a marker for PARP activity. Compared to the ***no RPE*** group, more photoreceptor cells in the ***FCCP***-treated retina showed PAR accumulation, correlating with decreased retinal NAD^+ levels (Figure 4E, F). Hence, ***FCCP***-induced oxidative stress may cause increased PARP activity and decreased NAD^+ levels, eventually interrupting the Krebs cycle, as evidenced by citrate accumulation.

bioRxiv preprint doi: https://doi.org/10.1101/2022.06.20.496788; this version posted June 21, 2022. The copyright holder for this preprint (which was not certified by peer review) is the author/funder. All rights reserved. No reuse allowed without permission.

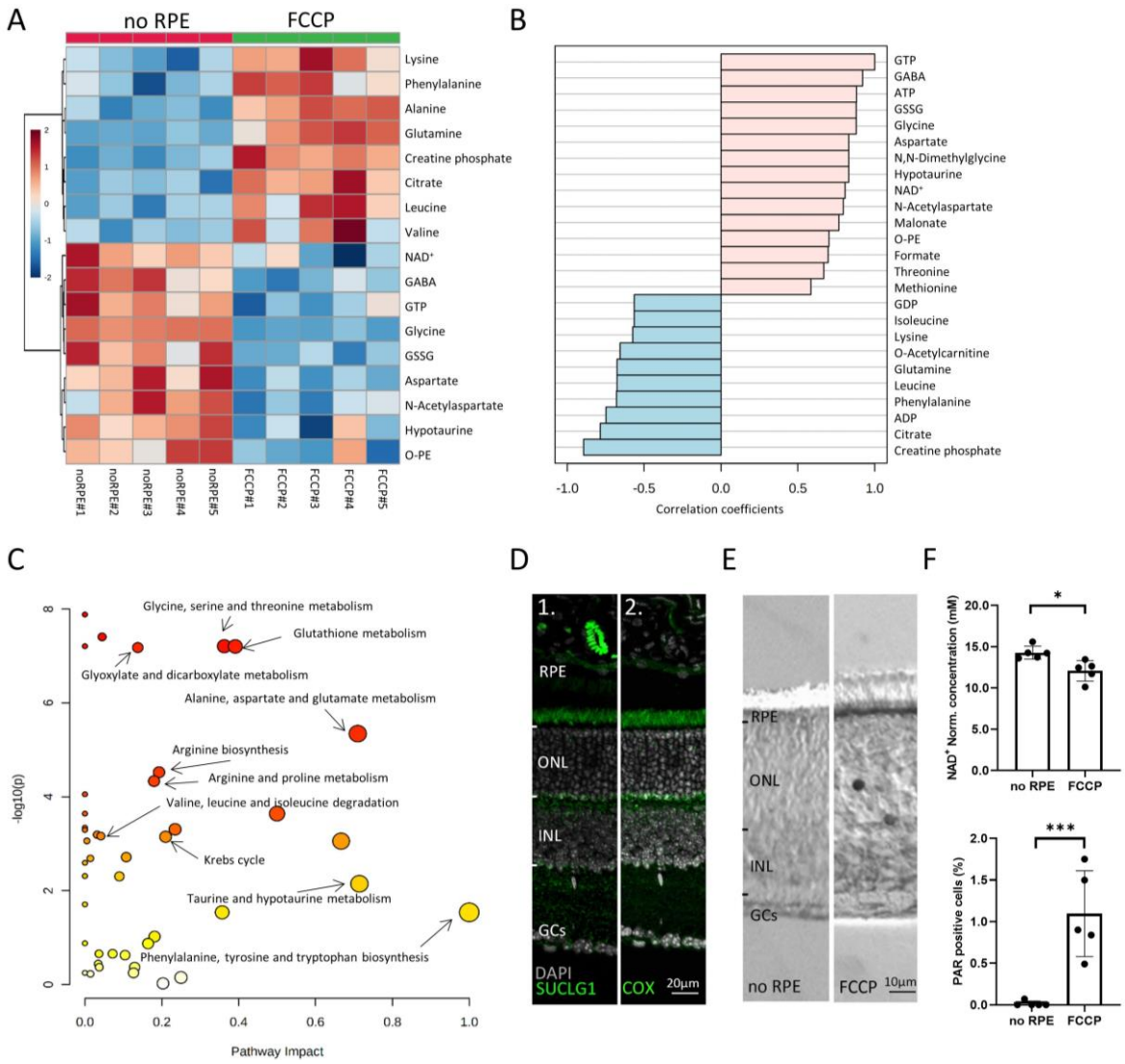

Figure 4. Comparison between *no RPE* and *FCCP* conditions. (**A**) Heatmap, based on unsupervised hierarchical cluster analysis by Ward's linkage, illustrating statistically significant metabolite changes (unpaired t-test, fold change > 1.2, raw p-value < 0.05). (**B**) Pattern hunter for guanosine triphosphate (GTP) showing the top 25 correlating compounds. Correlation coefficient given as Pearson r distance. (**C**) KEGG-based pathway analysis, comparison between no RPE and FCCP. (**D**) Immunofluorescence for succinate-CoA ligase-1 (SUCLG1, green) labelled photoreceptor inner segments and colocalized with COX. DAPI (grey) was used as a nuclear counterstain. (**E**) PAR positive photoreceptors (black) in the outer nuclear layer (ONL) of FCCP treated retina. (**F**) Compared to no RPE, NAD^+ levels were lower in the FCCP group, while the percentage of PAR positive cells was higher. Data represented as mean ± SD. *p* values: *** < 0.001, * < 0.05. See also Supplementary Figure 4.

Overall, the data from the ***no RPE*** to ***FCCP*** group comparison showed that disruption of OXPHOS led to AA accumulation, including lysine, phenylalanine, glutamine, leucine, and valine. Notably, alanine accumulation in the ***FCCP*** group was likely caused by ALT-dependent pyruvate transamination. By contrast, metabolites high in the ***no RPE*** group but low with ***FCCP*** treatment were probably generated via the Krebs cycle in the neuroretina. This concerned especially GTP, aspartate, and NAA.

bioRxiv preprint doi: https://doi.org/10.1101/2022.06.20.496788; this version posted June 21, 2022. The copyright holder for this preprint (which was not certified by peer review) is the author/funder. All rights reserved. No reuse allowed without permission.

Reduced retinal glucose uptake promotes anaplerotic metabolism

Since GLUT1 was predominantly expressed in the RPE, we assumed that the metabolic response to ***1,9-DDF*** treatment might resemble that of the ***no RPE*** situation. However, the patterns found between these two groups were very different (*cf*. Figure 2) revealing 28 significantly changed metabolites (Figure 5A; Supplementary Figure 5). When compared to the ***no RPE***, the ***1,9-DDF*** group showed changes in mitochondria and Krebs cycle associated metabolites (*e.g.*, high ATP, high formate, low BCAA). Conversely, the Cahill cycle product alanine and NAA were upregulated by ***1,9-DDF*** treatment. The pattern hunter analysis showed that metabolites formate, glutamate, taurine, and citrate were positively correlated with ATP, while, AMP, GMP, and BCAA were negatively correlated with ATP (Figure 5B).

The KEGG pathway analysis showed alanine, aspartate, and glutamate metabolism, glutathione metabolism and glycine, serine, and threonine metabolism among the three most affected pathways (Supplementary Figure 5B). Taken together, the depletion of BCAAs in the ***1,9-DDF*** treatment indicated that the retina used anaplerotic substrates to fuel the Krebs cycle and maintain ATP production.

bioRxiv preprint doi: https://doi.org/10.1101/2022.06.20.496788; this version posted June 21, 2022. The copyright holder for this preprint (which was not certified by peer review) is the author/funder. All rights reserved. No reuse allowed without permission.

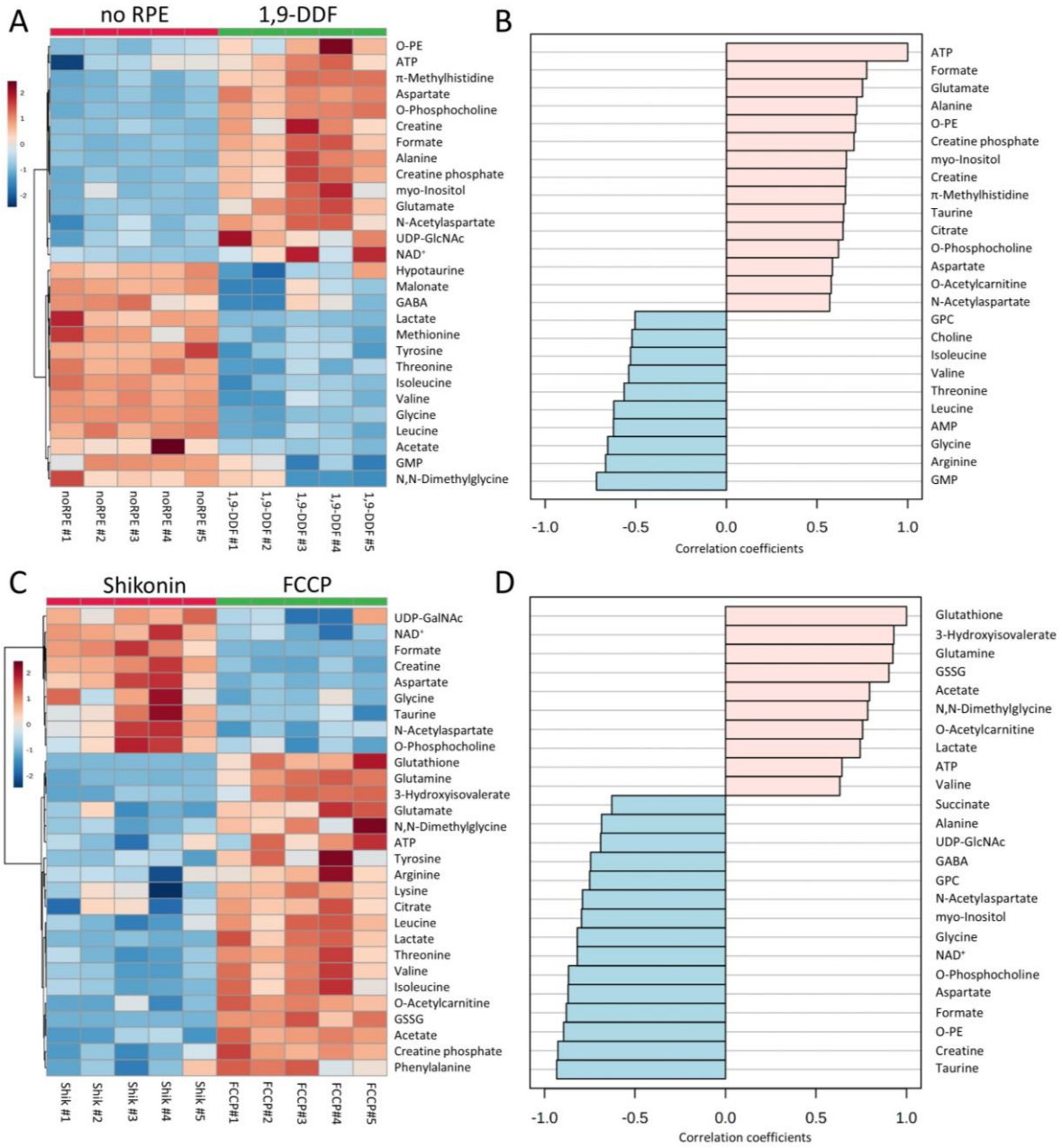

Figure 5. Metabolomic analysis of no RPE *vs*. 1,9-DDF treatment and Shikonin *vs*. FCCP treatment. Heatmap illustrating statistically significant metabolite changes (unpaired t-test, fold change (FC) > 1.2, raw *p* value < 0.05) for (**A**) no RPE *vs*. 1,9-DDF and (**C**) Shikonin *vs*. FCCP. Pattern hunter for (**B**) ATP and (**D**) glutathione, showing the top 25 correlating compounds. Correlation coefficient given as Pearson r distance. See also Supplementary Figures 5 and 6.

Inhibition of glycolysis strongly impacts retinal ATP production

We compared the ***Shikonin*** treatment, which inhibits the last step of glycolysis, to the ***FCCP*** treatment, which abolishes mitochondrial ATP synthesis (Figure 5C). Formate, aspartate, and NAA were increased in the ***Shikonin*** group. Conversely, higher amounts of GSH, GSSG, BCAA, threonine, and phenylalanine

bioRxiv preprint doi: https://doi.org/10.1101/2022.06.20.496788; this version posted June 21, 2022. The copyright holder for this preprint (which was not certified by peer review) is the author/funder. All rights reserved. No reuse allowed without permission.

after ***FCCP*** treatment indicated Krebs cycle interruption (Supplementary Figure 6). The production of lactate was higher with ***FCCP***- compared to ***Shikonin*** treatment, reflecting increased glycolysis to compensate for the loss of Krebs cycle-dependent ATP production. Metabolites connected to oxidative stress, such as GSSG and GSH, were also increased by ***FCCP*** treatment. Pattern hunter for metabolites correlated with glutathione found 3-hydroxyisovalerate, glutamine, GSSG, but also lactate and ATP, while succinate, alanine, and GABA were negatively correlated with GSH (Figure 5D). The subsequent pathway analysis identified arginine biosynthesis, alanine, aspartate, and glutamate metabolism, as well as glycolysis and gluconeogenesis as the most strongly regulated metabolic pathways (Supplementary Figure 6B).

Blocking glucose uptake and OXPHOS uncoupling reveal distinct rod and cone metabolism

The metabolic rate of cones is at least two times higher than that of rods[9]. The treatment with ***1,9-DDF*** resulted in near complete cone loss, while cones were fully preserved with ***FCCP*** treatment (*cf*. Figure 1). Therefore, we compared these two experimental groups with ***control*** to investigate the relative contributions of rods and cones to the metabolite patterns observed.

In this three-way comparison, 29 metabolite concentrations were significantly changed (Figure 6A; Supplementary Figure 7). The ***FCCP*** treatment reduced ATP and GTP levels, while lactate production was strongly increased, along with methionine and threonine. BCAAs, glutamine, phenylalanine and tyrosine also showed a significant upregulation with ***FCCP*** treatment. Interestingly, some metabolites like GSSG, serine, glutamate, alanine, NAD^+, and taurine displayed a pronounced increase in the ***1,9-DDF*** group when compared to either ***control*** or ***FCCP***. In addition, formate, aspartate, and myo-inositol were upregulated with ***1,9-DDF*** treatment, together with NAA and creatine. Finally, the comparison between the ***1,9-DDF*** and ***FCCP*** groups revealed highly increased levels of ATP and GTP, implying a strong activation of the Krebs cycle under ***1,9-DDF*** treatment.

bioRxiv preprint doi: https://doi.org/10.1101/2022.06.20.496788; this version posted June 21, 2022. The copyright holder for this preprint (which was not certified by peer review) is the author/funder. All rights reserved. No reuse allowed without permission.

A cell type-specific attribution of these metabolite patterns may be superseded by direct drug treatment effects. Using only metabolite changes in opposing directions from ***control*** to interpret different cellular compositions, we identified BCAAs, tyrosine, NAA, and ATP (glutamine with borderline significance; p = 0.66) (Supplementary Figure 7). BCAAs and tyrosine (and glutamine) exhibited low levels in the rod-rich ***1,9-DDF*** group and high levels in the cone-rich ***FCCP*** group, indicating that these metabolites might be consumed by rods or produced in cones. Vice versa, it can be assumed that aspartate and NAA were predominantly produced in rods.

To investigate the role of glutamine in retinal metabolism, we used immunofluorescence (Figure 6B). We confirmed a strong expression of glutamine synthase (GS) in MGCs[28]. Remarkably, the enzyme that hydrolyses glutamine to glutamate, glutaminase C (GAC) was prominently expressed in photoreceptor inner segments, photoreceptor synapses, and INL. Co-labelling with cone arrestin-3 (Arr3) revealed a particularly strong expression of GAC in cone inner segments, implying that cones use glutamine imported from MGCs as metabolic substrate.

bioRxiv preprint doi: https://doi.org/10.1101/2022.06.20.496788; this version posted June 21, 2022. The copyright holder for this preprint (which was not certified by peer review) is the author/funder. All rights reserved. No reuse allowed without permission.

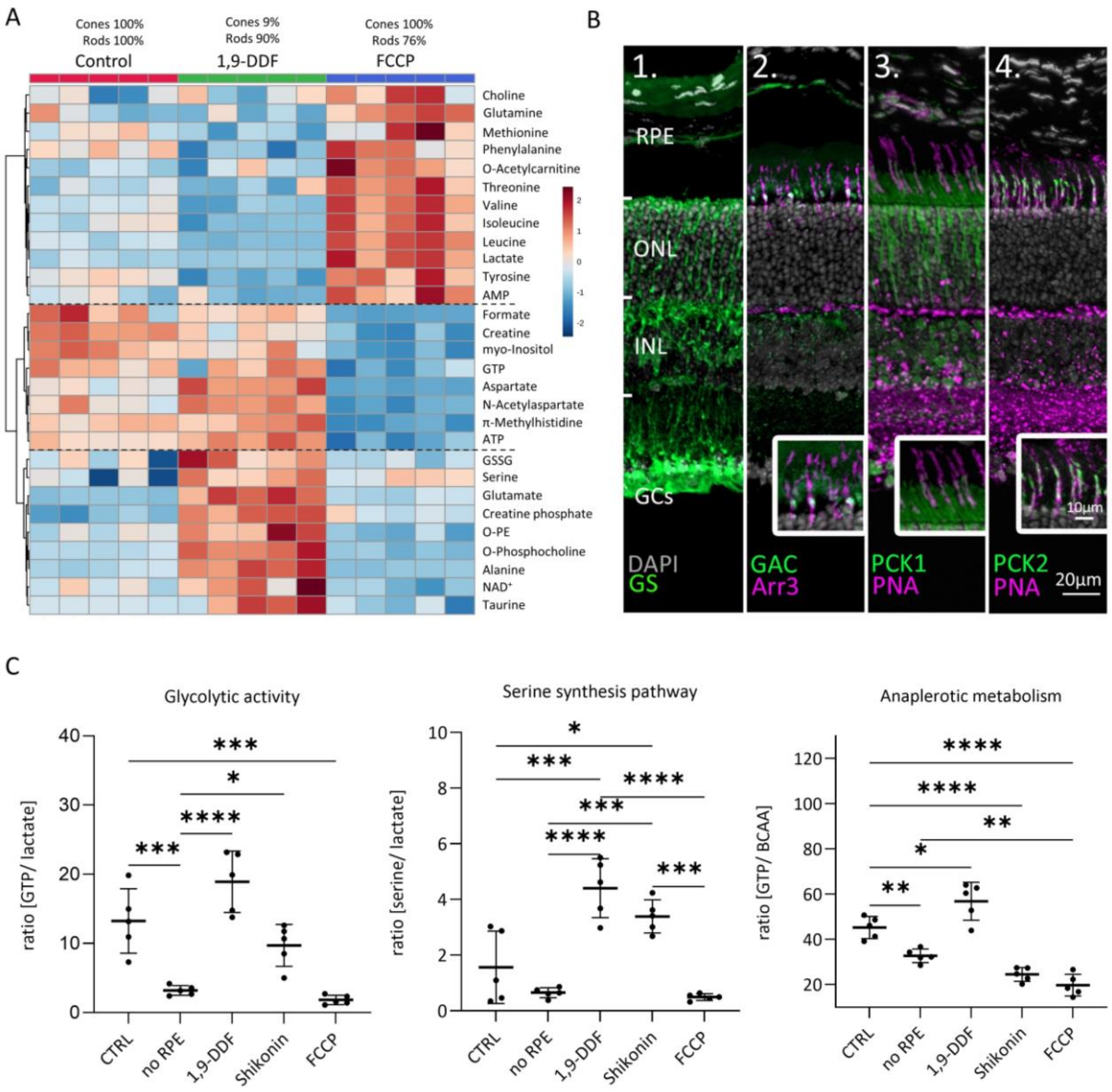

Figure 6. Metabolomic comparison between control, 1,9-DDF, and FCCP treatment. (**A**) Heatmap illustrating 29 statistically significant metabolite changes (parametric one-way ANOVA, Fisher's LSD post-hoc analysis). Three main clusters of metabolite changes were evident (dashed lines). (**B**) Immunostaining (green) for enzymes related to glutamine metabolism. DAPI (grey) was used as nuclear counterstain. (**B**1) Glutamine synthase (GS), (**B**2) glutaminase C (GAC); co-localization with cone-arrestin (Arr3; magenta). (**B**3) phosphoenolpyruvate carboxykinase 1 (PCK1) and (**B**4) PCK2, both co-localized with cone marker peanut-agglutinin (PNA). (**C**) Ratios between metabolites representing glycolysis (lactate *vs*. GTP), anaplerotic metabolism (GTP *vs*. BCAA), and serine synthesis pathway (serine *vs*. lactate). Data represented as individual data points with mean ± SD. Statistical comparison using one-way ANOVA, Tukey's multiple comparisons test; *p* values: **** < 0.0001, *** < 0.001, ** < 0.01 * < 0.05. See also Supplementary Figure 7.

bioRxiv preprint doi: https://doi.org/10.1101/2022.06.20.496788; this version posted June 21, 2022. The copyright holder for this preprint (which was not certified by peer review) is the author/funder. All rights reserved. No reuse allowed without permission.

Impact on glycolytic activity, serine synthesis pathway, and anaplerotic metabolism

To assess how the various experimental interventions affected retinal metabolism, we calculated the ratios for pathway specific metabolites (Figure 6C). GTP, when produced by SUCLG-1, is a marker for Krebs cycle activity, while lactate indicates glycolytic activity. In the ***no RPE*** group, the GTP-to-lactate ratio was significantly lower than in ***control***, indicating 4.1-times higher glycolytic activity. While in the ***1,9-DDF*** and ***Shikonin*** group the GTP-to-lactate ratios were not significantly different from ***control***, with ***FCCP*** treatment this ratio dropped to the lowest level, in line with a strong downregulation of Krebs cycle and concomitant upregulation of glycolysis.

We then calculated the ratio of serine to lactate as an indicator for serine synthesis pathway activity. Under ***control*** conditions, and in the ***no RPE*** and ***FCCP*** groups, this activity was rather low, while it was strongly increased by ***1,9-DDF*** and ***Shikonin*** treatment. In the ***Shikonin*** group, serine production from 3-phosphoglycerate and subsequent deamination to pyruvate may bypass the PKM2 block. Serine is also a precursor of phosphatidylserine, one of the three main cell membrane components. Together with a reduction of choline and high concentrations of myo-inositol, O-phosphocholine, and O-phosphoethanolamine, this may reflect high cell membrane synthesis under ***1,9-DDF*** treatment.

Finally, we used the ratio of GTP to BCAAs to investigate to what extent Krebs cycle activity was driven by anaplerotic metabolism. A comparatively low GTP to BCAA ratio in the ***no RPE*** situation showed that much of the GTP generated in the neuroretina likely came from anaplerotic substrates. While both ***Shikonin*** and ***FCCP*** treatment decreased BCAA use, ***1,9-DDF*** treatment increased anaplerotic metabolism.

bioRxiv preprint doi: https://doi.org/10.1101/2022.06.20.496788; this version posted June 21, 2022. The copyright holder for this preprint (which was not certified by peer review) is the author/funder. All rights reserved. No reuse allowed without permission.

Evidence for mini-Krebs cycle activity

Comparing the ratios of GTP to lactate with GTP to BCAA in the ***no RPE*** situation showed that a large proportion of the GTP produced in the neuroretina by SUCLG-1 was derived from anaplerotic substrates rather than from pyruvate. These substrates enter the Krebs cycle mostly at the level of α-ketoglutarate, suggesting that the neuroretinal Krebs cycle might not start with citrate. Instead, only the five steps from α-ketoglutarate to oxaloacetate would be employed, including the GTP-synthesizing step from succinyl-CoA to succinate (Figure 7A). A key step of this mini-Krebs cycle[29] is the transamination of oxaloacetate with glutamate by aspartate aminotransferase (AAT) to give α-ketoglutarate and aspartate, which is further acetylated to NAA. To investigate this possibility, we analysed eight metabolites associated with Krebs (citrate, succinate, fumarate, GTP) and mini-Krebs cycles (glutamine, glutamate, aspartate, NAA).

Hierarchical clustering showed similar patterns for aspartate and NAA in all experimental conditions (Figure 7B). Except for the ***FCCP*** treatment, the ratio of citrate/NAA was 0.5, indicating that the retina preferred the mini-Krebs cycle over the full Krebs cycle (Figure 7C). Immunolabelling for AAT – conventionally associated with muscle and liver metabolism[30,31] – found both AAT1 and AAT2 to be expressed in photoreceptor inner segments and cell bodies (Figure 7D). This confirmed that photoreceptors can execute the mini-Krebs cycle, while NAA production identified in the metabolomic data demonstrated that this cycle was indeed used.

bioRxiv preprint doi: https://doi.org/10.1101/2022.06.20.496788; this version posted June 21, 2022. The copyright holder for this preprint (which was not certified by peer review) is the author/funder. All rights reserved. No reuse allowed without permission.

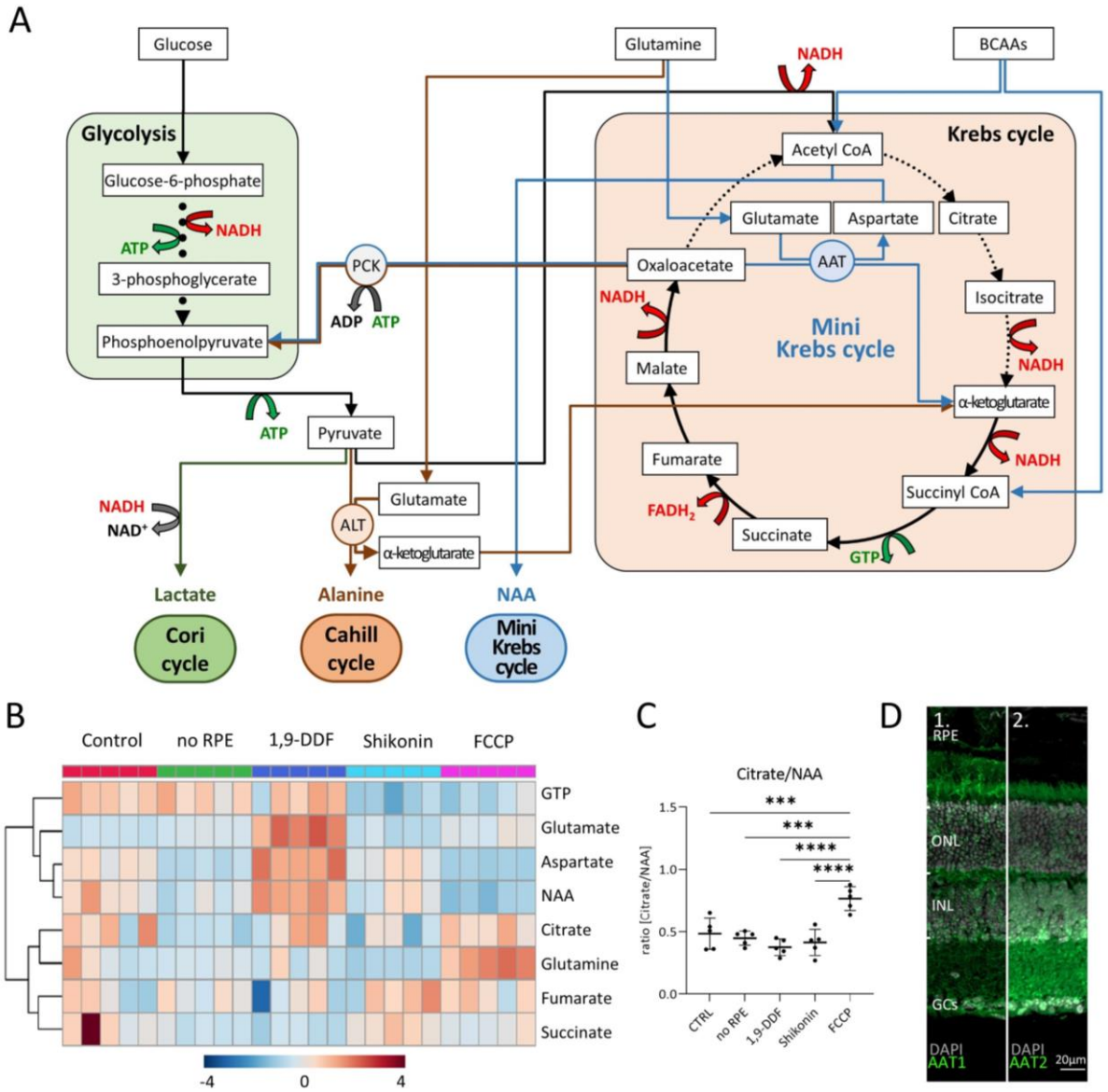

Figure 7. Metabolic pathways in the retina, key metabolites, and expression of aspartate amino transferase (AAT). (**A**) Overview of main metabolic pathways and metabolites. Execution of Cori- (green arrows), Cahill -(brown), or mini-Krebs- cycle (blue) releases the signature metabolites lactate, alanine, and N-acetylaspartate (NAA), respectively. Key enzymes of the Cahill- and mini-Krebs- cycle are alanine transaminase (ALT) and AAT. (**B**) Hierarchical clustering of eight metabolites connected to Krebs- and mini-Krebs- cycle. (**C**) Ratio NAA *vs*. citrate, representing full and mini-Krebs cycle. Data represented as ratio of individual data points with mean ± SD. (**D**) AAT-1 and -2 staining (green) with DAPI (grey) as nuclear counterstain.

Finally, we compared the energetic efficiencies of glycolysis, Krebs-, Cori-, Cahill-, and mini-Krebs- cycle (Figure 8). Using anaplerotic substrates in the Cahill- and mini-Krebs- cycle allows for far more efficient energy production compared to the Cori cycle. Moreover, mitochondrial PCK2 can regenerate pyruvate from oxaloacetate. Assuming that one mole of NADH/$FADH_2$ can be used to generate three moles of

bioRxiv preprint doi: https://doi.org/10.1101/2022.06.20.496788; this version posted June 21, 2022. The copyright holder for this preprint (which was not certified by peer review) is the author/funder. All rights reserved. No reuse allowed without permission.

ATP via OXPHOS, and depending on the exact stoichiometry of glutamate/BCAA input, the mini-Krebs cycle can deliver up to 18 moles of ATP and 2 moles of GTP per 3 carbon unit. Astonishingly, this is more than the 15 moles of ATP and 1 mole of GTP generated in the "full" Krebs cycle.

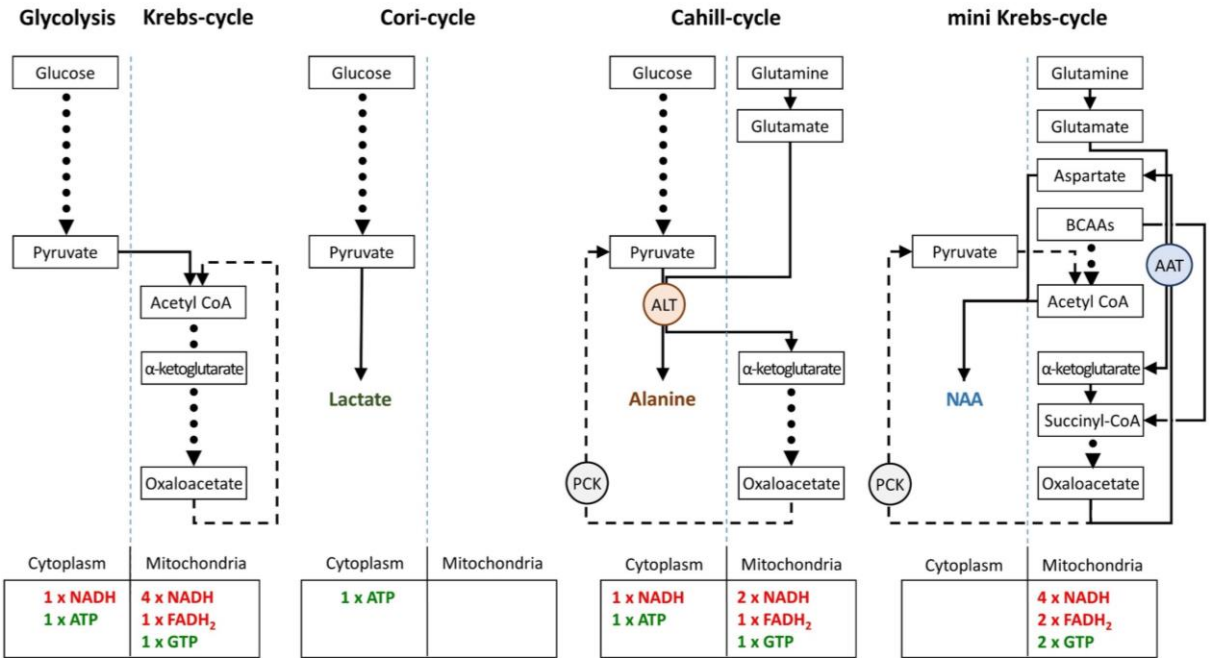

Figure 8. Comparison of metabolic pathways and their energetic efficiencies. Compared to the Cori-cycle, both Cahill- and mini-Krebs cycles are highly efficient. Their key enzymes – alanine transaminase (ALT) and aspartate amino transferase (AAT), respectively – generate alanine and aspartate/ N-acetylaspartate (NAA). Pyruvate carboxy kinase (PCK), either in cytoplasm or within mitochondria, may reconstitute pyruvate from oxalacetate. Note that energy output of each pathway was calculated based on input of pyruvate (three carbons) or glutamate/acetyl-CoA (three carbons).

Discussion

This study combines retinal cellular enzyme expression patterns with quantitative metabolomics. In an entirely controlled environment, this enabled a comprehensive assessment of retinal metabolism and allowed to analyse the impact of different experimental conditions on cell death and survival of retinal cells. As opposed to earlier works, our study highlights the crucial importance of OXPHOS and anaplerotic pathways for the maintenance and survival of rod and cone photoreceptors. Importantly, we show that photoreceptors can uncouple glycolysis and Krebs cycle using a NAA producing shunt, allowing optimal function of both pathways, and solving a long-standing problem in energy metabolism

bioRxiv preprint doi: https://doi.org/10.1101/2022.06.20.496788; this version posted June 21, 2022. The copyright holder for this preprint (which was not certified by peer review) is the author/funder. All rights reserved. No reuse allowed without permission.

research. Because of the ramifications for overall cellular physiology, these findings will be highly relevant for future therapy developments, for retinal diseases, as well as for neurodegenerative and metabolic diseases in general.

Under anaerobic conditions the production of lactate from glucose is a hallmark of skeletal muscle function. Here, pyruvate is reduced to lactate, which enters the bloodstream to serve as substrate for liver gluconeogenesis. Glucose can then cycle back to the muscle. This glucose-lactate cycle between muscle and liver was discovered in the 1930s and is referred to as Cori cycle[32]. The release of large amounts of lactate from isolated retina suggested that also the retina might use the Cori cycle, albeit under aerobic conditions[33]. Photoreceptors have thus been proposed to consume primarily glucose via aerobic glycolysis[10,11]. The resultant lactate would be used as fuel in the Krebs cycle by RPE and MGCs, generating ATP via OXPHOS. However, this hypothesis is contradicted by the high density of mitochondria in photoreceptor inner segments[34]. Moreover, key enzymes for Krebs cycle (CS, FH, SUCLG1) and OXPHOS (COX, ATP synthase γ) were strongly expressed in photoreceptors, but showed little or no expression in RPE or MGCs, in agreement with previous research[35]. When we cultured retina *without* RPE, as done by Warburg and others[3,4,10], we confirmed a strong lactate production. Yet, in retina cultured *with* RPE, lactate production was minor. Moreover, retina without RPE still produced large amounts of GTP, likely stemming from SUCLG1 activity and demonstrating Krebs cycle operation in photoreceptors. Neuroretina without RPE displayed reduced viability of both rod and cone photoreceptors, as well as an accumulation of BCAAs and lactate. In contrast, the block of glucose import into the RPE by treatment with 1,9-DDF[19] resulted in a depletion of BCAAs and other AAs, and an increase of retinal ATP, demonstrating a switch from glycolytic to anaplerotic metabolism[29]. We show that photoreceptors consume both glucose and anaplerotic substrates as fuels, and that retinal metabolism switches to aerobic glycolysis only in the absence of RPE. This switch is likely driven by increased glucose uptake. Normally, tight junction-coupled RPE cells form the outer blood-retinal barrier and prevent direct access of glucose to photoreceptors[36]. In the absence of RPE, photoreceptors expressing the high affinity/high capacity GLUT3 become “flooded” with glucose. The

bioRxiv preprint doi: https://doi.org/10.1101/2022.06.20.496788; this version posted June 21, 2022. The copyright holder for this preprint (which was not certified by peer review) is the author/funder. All rights reserved. No reuse allowed without permission.

resultant Crabtree effect then causes a shutdown of Krebs cycle activity[17,37,38]. Taken together, the high rates of retinal aerobic glycolysis first reported by Otto Warburg are likely an artefact of the absence of RPE, while intact retina strongly relies on OXPHOS for its energy production.

Treatment with FCCP revealed striking differences between rod and cone energy metabolism. FCCP eliminates the proton gradient between inner mitochondrial membrane and mitochondrial matrix, abolishing ATP synthesis[22]. Initially, FCCP may increase Krebs cycle activity to attempt restoration of mitochondrial proton gradient[39], increasing oxidative stress[40] and oxidative DNA damage. The resultant activation of PARP would deplete NAD^+, further aggravating metabolic stress[41]. Although FCCP had a strong toxic effect on rod photoreceptors, remarkably, cone photoreceptors were almost completely preserved. In striking contrast to the FCCP effect was that of the 1,9-DDF block on GLUT1[19]. Although GLUT1 was only expressed in the RPE, glucose entering the RPE is shuttled forward to photoreceptors[10]. Remarkably, with 1,9-DDF, over 90% of cones were lost, while the detrimental effect on rods was comparatively minor. These differential effects of FCCP and 1,9-DDF strongly suggest that glycolysis is sufficient and necessary for cone survival. Conversely, rods require OXPHOS for their survival, while glycolysis is of minor importance. In line with these interpretations, cone viability relative to rods was also strongly compromised in the no RPE situation, indicating that an intact blood-retinal barrier[36] and regulation of glucose access was important for cone survival. We note that GLUT2 may also contribute to photoreceptor glucose uptake[42].

The lactate-generating Cori cycle[32] is highly inefficient and in intact retina likely plays only a minor role. An efficient pathway is the glucose-alanine cycle, or Cahill cycle, in which pyruvate, instead of being reduced to lactate, is transaminated to alanine[25]. This preserves NADH and generates α-keto acids to fuel the Krebs cycle. The alanine generated enters the bloodstream and is taken up by the liver, where the ammonia is excreted in the form of urea, while the carbon backbone is used for gluconeogenesis. The key enzyme for the Cahill cycle is ALT, conventionally associated with muscle and liver[30,31]. Previously, ALT was found in glial cells of the honeybee retina[43], and ALT activity was detected in rat retinal tissue lysates[44]. In our study, the localization of ALT in photoreceptors and inner retinal neurons,

bioRxiv preprint doi: https://doi.org/10.1101/2022.06.20.496788; this version posted June 21, 2022. The copyright holder for this preprint (which was not certified by peer review) is the author/funder. All rights reserved. No reuse allowed without permission.

combined with our metabolomic datasets, demonstrated the operation of the Cahill cycle in the mammalian retina. Moreover, the expression of mitochondrial PCK2 in cones facilitates the efficient uncoupling of glycolysis from the Krebs cycle, suggesting that cones may use the Cahill cycle for very effective energy production.

MGCs are known for their uptake of extracellular glutamate and use for glutamine synthesis. In fact, in retinal histology, glutamate-aspartate transporter (GLAST) and glutamine synthase (GS) have been widely used as markers for MGCs[28,35,45]. Glutaminase C (GAC) converts glutamine back to glutamate, which may then serve as a substrate for the mini-Krebs cycle. We localized GAC in inner retinal neurons and photoreceptors, with a particularly strong expression in cone inner segments. Since ALT was strongly expressed in cone inner segments as well, cones can use glutaminolysis to obtain extra glutamate for pyruvate transamination in the Cahill cycle. This may also explain why the glycolysis inhibitor Shikonin reduced cone viability much less than that of rods.

The regeneration of the photoreceptor photopigment retinal is performed by the RPE[13]. Recently, retinal has been proposed to form a Schiff base adduct with taurine, which would act as a retinal carrier and buffer[46]. We found that retina cultured with RPE harboured high levels of taurine and low levels of hypotaurine, while retina without RPE displayed low levels of taurine and high levels of hypotaurine. Our taurine immunostaining found essentially no taurine in the RPE, while photoreceptor inner segments and synapses displayed very high taurine levels. Together, these findings suggest a hypotaurine-taurine shuttle between RPE and photoreceptors. In the RPE taurine can be reduced to hypotaurine and shuttled back to photoreceptors where oxidation by hypotaurine dehydrogenase[47,48] may reconstitute taurine, yielding additional NADH for OXPHOS. The net effect of this hypotaurine-taurine shuttle would be a transfer of reducing power from RPE to photoreceptors, boosting photoreceptor ATP production via OXPHOS.

A key problem in the understanding of cellular energy metabolism is the relationship between fast but inefficient glycolysis and slow but efficient Krebs cycle/OXPHOS[49,50]. Both pathways are coupled via pyruvate and the different metabolic flow rates reduce the efficiency of energy production, *e.g.*, via

bioRxiv preprint doi: https://doi.org/10.1101/2022.06.20.496788; this version posted June 21, 2022. The copyright holder for this preprint (which was not certified by peer review) is the author/funder. All rights reserved. No reuse allowed without permission.

feedback inhibition[51]. Pyruvate coupling is especially problematic in high and rapidly changing energy demand such as in neurons and photoreceptors[52]. Uncoupling glycolysis and Krebs cycle via the Cori cycle is extremely wasteful and likely insufficient to satisfy long-term photoreceptor energy demand. By comparison, the Cahill cycle delivers additional NADH when using pyruvate derived from glycolysis, and cones may use the Cahill cycle for uncoupling from glycolysis. An alternative pathway is the mini-Krebs cycle, essentially an oxalacetate to α-ketoglutarate shunt[29]. This cycle uses glutamate, glutamine, and BCAAs as fuels to run mitochondrial respiration independent of glycolysis. The key step of the mini-Krebs cycle is the transamination of oxaloacetate/glutamate to aspartate/α-ketoglutarate by AAT. α-ketoglutarate is then metabolized to oxaloacetate, generating NADH, $FADH_2$, and GTP. Acetyl-CoA generated from BCAAs or pyruvate is used to create NAA, the end product of the mini-Krebs cycle. We found mitochondrial AAT2 to be expressed in rod inner segments, in agreement with an early cytochemical study[53]. This indicates that the mini-Krebs cycle is used primarily by rods, explaining their selective vulnerability to FCCP treatment. Crucially, the mini-Krebs cycle is more energy-efficient than the Cahill cycle and generates NAA instead of alanine as net product. Both metabolites serve the purpose of disposing of excess ammonia originating from AA input[54,55]. NAA in the human brain is one of the most abundant metabolites and is routinely used in clinical MRI diagnosis to visualize brain health[56,57]. While different functions have been hypothesized for NAA[58,59], our work proposes NAA as a signature metabolite for the mini-Krebs cycle. Indeed, a recent study using Raman spectroscopy imaging detected high levels of NAA in the human retina, demonstrating *in vivo* use of this cycle[60]. Importantly, the 6-step mini-Krebs cycle is significantly faster than the 10-step Krebs cycle[29] and is uncoupled from glycolysis. In rods, PCK1 may allow to replenish cytoplasmic acetyl-CoA pools from oxaloacetate, if BCAA-derived input was insufficient.

Overall, the different pathways outlined here provide photoreceptor cells with a remarkable versatility and flexibility, allowing to dynamically adapt the timing and quantitative output of energy metabolism. The differences between rod and cone metabolism may be related to their response kinetics and sensitivities. Importantly, our study highlights the significance of the Krebs cycle and OXPHOS for rods,

bioRxiv preprint doi: https://doi.org/10.1101/2022.06.20.496788; this version posted June 21, 2022. The copyright holder for this preprint (which was not certified by peer review) is the author/funder. All rights reserved. No reuse allowed without permission.

as well as the strong reliance of cones on glycolysis. We demonstrate the ability of photoreceptors to flexibly uncouple glycolysis from mitochondrial respiration, allowing both processes to run at optimum, and producing the characteristic signature metabolites lactate (Cori cycle), alanine (Cahill cycle), and NAA (mini-Krebs cycle). These metabolites can reveal energy or disease status and could serve as readout and guide for the design of novel therapeutic interventions. Given the general importance of energy metabolism, the significance of our findings extends beyond the retina, for instance, to other neurodegenerative and metabolic diseases.

bioRxiv preprint doi: https://doi.org/10.1101/2022.06.20.496788; this version posted June 21, 2022. The copyright holder for this preprint (which was not certified by peer review) is the author/funder. All rights reserved. No reuse allowed without permission.

Acknowledgements

We thank N. Rieger and M. Owczorz for first-rate technical support and James B. Hurley (University of Washington) for helpful comments and suggestions. This work was funded by the ProRetina Foundation, the Zinke heritage foundation, the Werner Siemens Foundation, the Chinese scholarship council (CSC), ANID-FONDECYT No. 1210790 (OS) and PhD grant BECAS CHILE/2018 -21180443 (VC).

Author Contributions

Conceptualization, Y.C., L.Z., F.P.D., and C.T.; Methodology, Y.C., L.Z., F.P.D., and C.T.; Investigation, Y.C., L.Z., S.Y., F.P.D., and C.T.; Writing – original draft, Y.C., L.Z., F.P.D., and C.T.; Writing – Review & Editing, F.W.H., O.S. and V.C.; Supervision, F.P.D., and C.T.; Funding acquisition, F.P.D., and C.T.

Declaration of Interests

The authors declare no competing financial interests.

bioRxiv preprint doi: https://doi.org/10.1101/2022.06.20.496788; this version posted June 21, 2022. The copyright holder for this preprint (which was not certified by peer review) is the author/funder. All rights reserved. No reuse allowed without permission.

MATERIALS AND METHODS

RESOURCE AVAILABLITY

Lead contact

Further information and requests for resources and reagents should be directed to and will be fulfilled by the lead contact, François Paquet-Durand (francois.paquet-durand@klinikum.uni-tuebingen.de).

Materials availability

The study did not generate new unique reagents.

Data and Code availability

Any additional information required to reanalyze the data reported in this paper is available from the lead contact upon request. This paper does not report original code.

METHOD DETAILS

Animals

C3H wild-type (WT) mice were used[61]. All efforts were made to minimize the number of animals used and their suffering. Animals were housed under standard white cyclic lighting, had free access to food and water, and were used irrespective of gender. Protocols compliant with the German law on animal protection were reviewed and approved by the ‘‘Einrichtung fur Tierschutz, Tierärztlichen Dienst und Labortierkunde’’ of the University of Tübingen and were following the association for research in vision and ophthalmology (ARVO) statement for the use of animals in vision research. Animals were not assigned to experimental groups prior to their sacrifice.

bioRxiv preprint doi: https://doi.org/10.1101/2022.06.20.496788; this version posted June 21, 2022. The copyright holder for this preprint (which was not certified by peer review) is the author/funder. All rights reserved. No reuse allowed without permission.

Retinal explant cultures

The retinal explantation procedure and long-term cultivation in defined medium, free of serum and antibiotics, is described in detail in[18]. Briefly, mice were decapitated at postnatal day (P) 9 and the heads cleaned with 70% ethanol. The eyes were removed under aseptic conditions, and placed into R16 basal medium (BM; Gibco, Paisley, UK), washed for 5 min, followed by a 15 min incubation in 0.12% Proteinase K (Sigma-Aldrich Chemie GmbH, Taufkirchen, Germany; P6556) at 37°C to predigest the sclera and to allow for an easy separation of the retina together with its retinal pigment epithelium (RPE). Then, the eyes were placed for 5 min in BM with 10% foetal calf serum (FCS) to deactivate Proteinase K. In the case of no RPE explants, the retina was explanted directly, without Proteinase K pre-treatment and FCS deactivation. Under the microscope and sterile conditions, the anterior segment, lens, and vitreous body were carefully removed from the eyeballs, the optic nerve was cut, and the retinas were removed from the sclera. Then four incisions were made into the retina to give a flat, clover leaf like structure that was transferred to a culturing membrane (sterile 24 mm insert with 0.4 µm polycarbonate membrane, Corning-Costar, New York, NY, USA), with the ganglion cell layer facing up. Subsequently, culturing membranes were placed in six-well culture plates (BD Biosciences, San Jose, CA, USA) and incubated in 1 ml of R16 complete medium (CM) with supplements [62], at 37°C, in a humidified incubator with 5% CO2. From P9 to P11 cultures were kept in CM, treatments with 50µM 1,9-DDF and 4µM Shikonin were applied from P11 until P15, while 5µM FCCP treatment was applied from P13 to P15. The medium was changed every 2 days.

Culturing was stopped by 45 min fixation in 4% paraformaldehyde (PFA), cryoprotected with graded sucrose solutions containing 10, 20, and 30% sucrose and then embedded in Tissue-Tek O.C.T. compound (Sakura Finetek Europe, Alphen aan den Rijn, Netherlands). Tissue sections of 12 µm were prepared using Thermo Scientific NX50 microtome (Thermo Scientific, Waltham, MA) and thaw-mounted onto Superfrost Plus glass slides (R. Langenbrinck, Emmendingen, Germany).

bioRxiv preprint doi: https://doi.org/10.1101/2022.06.20.496788; this version posted June 21, 2022. The copyright holder for this preprint (which was not certified by peer review) is the author/funder. All rights reserved. No reuse allowed without permission.

Cell death detection (TUNEL assay)

Fixed slides were dried at 37°C for 30 min and washed in phosphate buffered saline (PBS) solution at room temperature (RT), for 15 min. Afterwards, the slides were placed in TRIS buffer with proteinase K at 37°C for 5 min to inactivate nucleases. The slides were then washed with TRIS buffer (10 mM TRIS-HCL, pH 7.4), 3 times for 5 minutes each. Subsequently, the slides were placed in ethanol-acetic acid mixture (70:30) at -20°C for 5 min followed by 3 washes in TRIS buffer and incubation in blocking solution (10% normal goat serum, 1% bovine serum albumin, 1% fish gelatine in 0.1% PBS-Triton X100) for 1h at RT. Lastly, the slides were placed in the terminal dUTP-nick-end labelling (TUNEL) solution (labelling with either fluorescein or tetra-methyl-rhodamine; Roche Diagnostics GmbH, Mannheim, Germany) in 37°C for 1 h and mounted with Vectashield with DAPI (Vector, Burlingame, CA, USA) thereafter.

Immunofluorescence

Fixed slides were dried at 37°C for 30 min and rehydrated for 10 min in PBS at RT. For immunofluorescent labelling, the slides were incubated with blocking solution (10% normal goat serum, 1% bovine serum albumin in 0.3% PBS-Triton X 100) for 1 h at RT. The primary antibodies were diluted (see table 1) in blocking solution and incubated at 4°C overnight. The slides were then washed with PBS, 3 times for 10 min each. Subsequently, the secondary antibody, diluted in PBS (see table 1), was applied to the slides, and incubated for 1 h at RT. Lastly, the slides were washed with PBS and mounted with Vectashield with DAPI (Vector).

bioRxiv preprint doi: https://doi.org/10.1101/2022.06.20.496788; this version posted June 21, 2022. The copyright holder for this preprint (which was not certified by peer review) is the author/funder. All rights reserved. No reuse allowed without permission.

REAGENT or RESOURCE	SOURCE	IDENTIFIER
Antibodies		
Mouse monoclonal anti-RPE65	Thermo Fisher Scientific	Cat# MA5-16042, RRID: AB_11151857
Rabbit polyclonal anti-GLUT1	Abcam	Cat# ab652, RRID:AB_305540
Rabbit polyclonal anti-GLUT3	Abcam	Cat# ab41525, RRID:AB_732609
Rabbit monocolonal anti-PKM1	Cell Signaling Technology	Cat# 7067, RRID: AB_2715534
Rabbit monocolonal anti-PKM2	Cell Signaling Technology	Cat# 4053, RRID: AB_1904096
Mouse monoclonal anti-Cytochrome C	Molecular Probes	Cat# A-6403, RRID: AB_221582
Rabbit polyclonal anti-Cone arrestin	Sigma-Aldrich	Cat# AB15282; RRID:AB_1163387
Rabbit polyclonal anti-Citrate synthase	GeneTex	Cat# GTX110624, RRID: AB_1950045
Rabbit polyclonal anti-ATP synthase gamma	GeneTex	Cat# GTX114275S, RRID: AB_10726795
Rabbit polyclonal anti- Fumarate hydratase	GeneTex	Cat# GTX109877, RRID: AB_1950283
Rabbit polyclonal anti- Taurine	Abcam	Cat# ab9448, RRID: AB_307261
Rabbit monocolonal anti-Alanine transaminase (AAT1)	Abcam	Cat# ab202083, RRID:AB_2915976
Rabbit polyclonal anti-SUCLG1	Novus Biologicals	Cat# NBP1-32728, RRID: AB_2286802
Rabbit polyclonal anti-Glutamine synthetase	Abcam	Cat# ab73593, RRID: AB_2247588
Rabbit polyclonal anti- Glutaminase C (GAC)	GeneTex	Cat# GTX131263, RRID: AB_2886452
Rabbit polyclonal anti- PCK1	Affinity Biosciences	Cat# DF6770, RRID:AB_2838732
Rabbit monocolonal anti- PCK2	Novus Biologicals	Cat# NBP2-75610 RRID: AB_2915974
Peanut agglutinin (PNA)	Vector laboratories	Cat# FL-1071, RRID:AB_2315097
Rabbit polyclonal anti- Aspartate aminotransferase1	Abcam	Cat# ab221939, RRID: AB_2915980
Rabbit polyclonal anti- FABP-1 (Aspartate aminotransferase2)	Abcam	Cat# ab153924, RRID:AB_2915981

Table 1: Primary and secondary antibodies used in the study, providers, and dilutions.

Microscopy, cell counting, and statistical analysis

Fluorescence microscopy was performed with a Z1 Apotome microscope equipped with a Zeiss Axiocam digital camera (Zeiss, Oberkochen, Germany). Images were captured using Zen software (Zeiss) and the Z-stack function (14-bit depth, 2752*2208 pixels, pixel size = 0.227 µm, 9 Z-planes at 1 µm

bioRxiv preprint doi: https://doi.org/10.1101/2022.06.20.496788; this version posted June 21, 2022. The copyright holder for this preprint (which was not certified by peer review) is the author/funder. All rights reserved. No reuse allowed without permission.

steps). The raw images were converted into maximum intensity projections using Zen software and saved as TIFF files.

Photoreceptors stained by the TUNEL assay were counted manually on three images per explant, the average cell number in a given ONL area was estimated based on DAPI staining and used to calculate the percentage of TUNEL positive cells. Adobe Photoshop CS6 (Adobe Systems Incorporated, San Jose, CA) and Adobe Illustrator CC 2019 software was used for primary image processing. All data given represent the means and standard deviation from at least 5 different animals. Statistical comparisons between experimental groups were made using Student´s paired t-test (*cf*. Figure 1) or ANOVA and multiple comparisons correction (*cf*. Figures 1) using Graph Pad Prism 9.1 for Windows (Graph Pad Software, La Jolla, CA). Levels of significance were as follows: * = $p < 0.05$; ** = $p < 0.01$; *** = $p < 0.001$.

Metabolite extraction

After retinal explant culture, the tissue was quickly transferred into 80% methanol / 20% ethanol, snap-frozen in liquid nitrogen, and further subjected to metabolite extraction via ultra-sonication (Covaris E220 Evolution, Woburn, USA). Retinal tissue was collected in 400 µL of methanol (LC-MS grade), transferred to the 2 mL glass Covaris system-compatible tubes and 800 µL of methyl-*tert*-butyl ether (MTBE) was added and thoroughly mixed. After the extraction, 400 µL of ultrapure water were added for two-phase liquid separation. The aqueous phase was separated and evaporated to dryness.

Sample preparation for ^{1}H-NMR spectroscopy measurements and data analysis

Dried metabolite pellets were resuspended in a deuterated phosphate buffer (pH corrected for 7.4) with 1 mM of 3-(trimethylsilyl) propionic-2,2,3,3-d4 acid sodium salt (TSP) as internal standard. NMR spectra were recorded at 298 K on a 14.1 Tesla ultra-shielded NMR spectrometer at 600 MHz proton frequency (Avance III HD, Bruker BioSpin, Germany) equipped with a triple resonance 1.7 mm room

bioRxiv preprint doi: https://doi.org/10.1101/2022.06.20.496788; this version posted June 21, 2022. The copyright holder for this preprint (which was not certified by peer review) is the author/funder. All rights reserved. No reuse allowed without permission.

temperature micro probe. Short zero-go (zg), 1D nuclear Overhauser effect spectroscopy (NOESY) and Carr-Purcell-Meiboom-Gill (CPMG, 1024 scans) pulse programs were used for spectra acquisition. Spectra were processed with Bruker TopSpin 3.6.1 software (Bruker BioSpin, Ettlingen, Germany).

Quantification and statistical analysis

Metabolite assignments for quantification were performed with ChenomX NMR Suite 8.5 (Chenomx Inc., Edmonton, Canada). Statistical analysis was performed with MetaboAnalyst 5.0 platform (https://www.metaboanalyst.ca [63]) and GraphPad Prism 9.1.0 software (GraphPad Software, San Diego, CA, USA). Metabolite pathway analysis and pathway impact values were based on Kyoto Encyclopaedia of Genes and Genomes (KEGG) pathway database.

bioRxiv preprint doi: https://doi.org/10.1101/2022.06.20.496788; this version posted June 21, 2022. The copyright holder for this preprint (which was not certified by peer review) is the author/funder. All rights reserved. No reuse allowed without permission.

References

1. Country, M.W. Retinal metabolism: A comparative look at energetics in the retina. *Brain Res* **1672**, 50-57 (2017).
2. Wong-Riley, M.T. Energy metabolism of the visual system. *Eye Brain* **2**, 99-116 (2010).
3. Winkler, B.S. Glycolytic and oxidative metabolism in relation to retinal function. *J Gen Physiol* **77**, 667-692 (1981).
4. Warburg, O. The Metabolism of Carcinoma Cells. *The Journal of Cancer Research* **9**, 148-163 (1925).
5. Okawa, H., Sampath, A.P., Laughlin, S.B. & Fain, G.L. ATP consumption by mammalian rod photoreceptors in darkness and in light. *Curr Biol* **18**, 1917-1921 (2008).
6. Ames, A., 3rd. Energy requirements of CNS cells as related to their function and to their vulnerability to ischemia: a commentary based on studies on retina. *Can J Physiol Pharmacol* **70 Suppl**, S158-164 (1992).
7. Chinchore, Y., Begaj, T., Wu, D., Drokhlyansky, E. & Cepko, C.L. Glycolytic reliance promotes anabolism in photoreceptors. *Elife* **6**(2017).
8. Young, R.W. The renewal of photoreceptor cell outer segments. *J Cell Biol* **33**, 61-72 (1967).
9. Ingram, N.T., Fain, G.L. & Sampath, A.P. Elevated energy requirement of cone photoreceptors. *Proceedings of the National Academy of Sciences* **117**, 19599-19603 (2020).
10. Kanow, M.A.*, et al.* Biochemical adaptations of the retina and retinal pigment epithelium support a metabolic ecosystem in the vertebrate eye. *Elife* **6**(2017).
11. Sinha, T., Naash, M.I. & Al-Ubaidi, M.R. The Symbiotic Relationship between the Neural Retina and Retinal Pigment Epithelium Is Supported by Utilizing Differential Metabolic Pathways. *iScience* **23**, 101004 (2020).
12. Viegas, F.O. & Neuhauss, S.C.F. A Metabolic Landscape for Maintaining Retina Integrity and Function. *Front Mol Neurosci* **14**, 656000 (2021).
13. Redmond, T.M.*, et al.* Rpe65 is necessary for production of 11-cis-vitamin A in the retinal visual cycle. *Nat Genet* **20**, 344-351 (1998).
14. Swarup, A.*, et al.* Modulating GLUT1 expression in retinal pigment epithelium decreases glucose levels in the retina: impact on photoreceptors and Müller glial cells. *Am J Physiol Cell Physiol* **316**, C121-c133 (2019).
15. Takata, K., Kasahara, T., Kasahara, M., Ezaki, O. & Hirano, H. Erythrocyte/HepG2-type glucose transporter is concentrated in cells of blood-tissue barriers. *Biochem Biophys Res Commun* **173**, 67-73 (1990).
16. Takata, K., Kasahara, T., Kasahara, M., Ezaki, O. & Hirano, H. Ultracytochemical localization of the erythrocyte/HepG2-type glucose transporter (GLUT1) in cells of the blood-retinal barrier in the rat. *Invest Ophthalmol Vis Sci* **33**, 377-383 (1992).
17. Simpson, I.A.*, et al.* The facilitative glucose transporter GLUT3: 20 years of distinction. *Am J Physiol Endocrinol Metab* **295**, E242-253 (2008).
18. Belhadj, S.*, et al.* Long-Term, Serum-Free Cultivation of Organotypic Mouse Retina Explants with Intact Retinal Pigment Epithelium. *J Vis Exp* (2020).
19. Joost, H.G., Habberfield, A.D., Simpson, I.A., Laurenza, A. & Seamon, K.B. Activation of adenylate cyclase and inhibition of glucose transport in rat adipocytes by forskolin analogues: structural determinants for distinct sites of action. *Mol Pharmacol* **33**, 449-453 (1988).
20. Chen, J.*, et al.* Shikonin and its analogs inhibit cancer cell glycolysis by targeting tumor pyruvate kinase-M2. *Oncogene* **30**, 4297-4306 (2011).
21. Zhao, X.*, et al.* Shikonin Inhibits Tumor Growth in Mice by Suppressing Pyruvate Kinase M2-mediated Aerobic Glycolysis. *Scientific Reports* **8**, 14517 (2018).
22. Kessler, R.J., Tyson, C.A. & Green, D.E. Mechanism of uncoupling in mitochondria: uncouplers as ionophores for cycling cations and protons. *Proc Natl Acad Sci U S A* **73**, 3141-3145 (1976).

bioRxiv preprint doi: https://doi.org/10.1101/2022.06.20.496788; this version posted June 21, 2022. The copyright holder for this preprint (which was not certified by peer review) is the author/funder. All rights reserved. No reuse allowed without permission.

23. Ortin-Martinez, A., *et al.* Number and distribution of mouse retinal cone photoreceptors: differences between an albino (Swiss) and a pigmented (C57/BL6) strain. *PloS one* **9**, e102392 (2014).
24. Jeon, C.J., Strettoi, E. & Masland, R.H. The major cell populations of the mouse retina. *J Neurosci* **18**, 8936-8946 (1998).
25. Felig, P. The glucose-alanine cycle. *Metabolism* **22**, 179-207 (1973).
26. Bai, P. Biology of Poly(ADP-Ribose) Polymerases: The Factotums of Cell Maintenance. *Mol Cell* **58**, 947-958 (2015).
27. Paquet-Durand, F., *et al.* Excessive activation of poly(ADP-ribose) polymerase contributes to inherited photoreceptor degeneration in the retinal degeneration 1 mouse. *J Neurosci* **27**, 10311-10319 (2007).
28. Riepe, R.E. & Norenburg, M.D. Müller cell localisation of glutamine synthetase in rat retina. *Nature* **268**, 654-655 (1977).
29. Yudkoff, M., Nelson, D., Daikhin, Y. & Erecińska, M. Tricarboxylic acid cycle in rat brain synaptosomes. Fluxes and interactions with aspartate aminotransferase and malate/aspartate shuttle. *J Biol Chem* **269**, 27414-27420 (1994).
30. Nathwani, R.A., Pais, S., Reynolds, T.B. & Kaplowitz, N. Serum alanine aminotransferase in skeletal muscle diseases. *Hepatology* **41**, 380-382 (2005).
31. Kim, W.R., Flamm, S.L., Di Bisceglie, A.M. & Bodenheimer, H.C. Serum activity of alanine aminotransferase (ALT) as an indicator of health and disease. *Hepatology* **47**, 1363-1370 (2008).
32. Cori, C.F. & Cori, G.T. Carbohydrate metabolism. *Annu Rev Biochem* **15**, 193-218 (1946).
33. Rajala, R.V.S. Aerobic Glycolysis in the Retina: Functional Roles of Pyruvate Kinase Isoforms. *Frontiers in Cell and Developmental Biology* **8**(2020).
34. Giarmarco, M.M., *et al.* Daily mitochondrial dynamics in cone photoreceptors. *Proc Natl Acad Sci U S A* **117**, 28816-28827 (2020).
35. Rueda, E.M., *et al.* The cellular and compartmental profile of mouse retinal glycolysis, tricarboxylic acid cycle, oxidative phosphorylation, and ~P transferring kinases. *Mol Vis* **22**, 847-885 (2016).
36. O'Leary, F. & Campbell, M. The blood-retina barrier in health and disease. *Febs j* (2021).
37. Diaz-Ruiz, R., Rigoulet, M. & Devin, A. The Warburg and Crabtree effects: On the origin of cancer cell energy metabolism and of yeast glucose repression. *Biochimica et Biophysica Acta (BBA) - Bioenergetics* **1807**, 568-576 (2011).
38. Crabtree, H.G. Observations on the carbohydrate metabolism of tumours. *Biochem J* **23**, 536-545 (1929).
39. Balcke, G.U., *et al.* Linking energy metabolism to dysfunctions in mitochondrial respiration--a metabolomics in vitro approach. *Toxicol Lett* **203**, 200-209 (2011).
40. Dugan, L.L., *et al.* Mitochondrial production of reactive oxygen species in cortical neurons following exposure to N-methyl-D-aspartate. *J Neurosci* **15**, 6377-6388 (1995).
41. Schreiber, V., Dantzer, F., Ame, J.C. & de Murcia, G. Poly(ADP-ribose): novel functions for an old molecule. *Nat Rev Mol Cell Biol* **7**, 517-528 (2006).
42. Yang, M., *et al.* Expression of glucose transporter-2 in murine retina: Evidence for glucose transport from horizontal cells to photoreceptor synapses. *J Neurochem* **160**, 283-296 (2022).
43. Tsacopoulos, M., Veuthey, A.L., Saravelos, S.G., Perrottet, P. & Tsoupras, G. Glial cells transform glucose to alanine, which fuels the neurons in the honeybee retina. *J Neurosci* **14**, 1339-1351 (1994).
44. LaNoue, K.F., *et al.* Role of specific aminotransferases in de novo glutamate synthesis and redox shuttling in the retina. *J Neurosci Res* **66**, 914-922 (2001).
45. Danbolt, N.C. Glutamate uptake. *Prog Neurobiol* **65**, 1-105 (2001).
46. Kim, H.J., Zhao, J. & Sparrow, J.R. Vitamin A aldehyde-taurine adduct and the visual cycle. *Proceedings of the National Academy of Sciences* **117**, 24867-24875 (2020).

bioRxiv preprint doi: https://doi.org/10.1101/2022.06.20.496788; this version posted June 21, 2022. The copyright holder for this preprint (which was not certified by peer review) is the author/funder. All rights reserved. No reuse allowed without permission.

47. Veeravalli, S.*, et al.* Flavin-Containing Monooxygenase 1 Catalyzes the Production of Taurine from Hypotaurine. *Drug Metab Dispos* **48**, 378-385 (2020).
48. Sumizu, K. Oxidation of hypotaurine in rat liver. *Biochim Biophys Acta* **63**, 210-212 (1962).
49. Zheng, J. Energy metabolism of cancer: Glycolysis versus oxidative phosphorylation (Review). *Oncol Lett* **4**, 1151-1157 (2012).
50. Pfeiffer, T., Schuster, S. & Bonhoeffer, S. Cooperation and competition in the evolution of ATP-producing pathways. *Science* **292**, 504-507 (2001).
51. Lai, J.C. & Behar, K.L. Glycolysis-citric acid cycle interrelation: a new approach and some insights in cellular and subcellular compartmentation. *Dev Neurosci* **15**, 181-193 (1993).
52. Du, J.*, et al.* Phototransduction Influences Metabolic Flux and Nucleotide Metabolism in Mouse Retina. *J Biol Chem* **291**, 4698-4710 (2016).
53. Gebhard, R. Cytochemical demonstration of aspartate aminotransferase activity in the rat retina. *Brain Res* **539**, 337-341 (1991).
54. Moffett, J.R., Ross, B., Arun, P., Madhavarao, C.N. & Namboodiri, A.M.A. N-Acetylaspartate in the CNS: from neurodiagnostics to neurobiology. *Progress in neurobiology* **81**, 89-131 (2007).
55. Dadsetan, S.*, et al.* Brain alanine formation as an ammonia-scavenging pathway during hyperammonemia: effects of glutamine synthetase inhibition in rats and astrocyte-neuron co-cultures. *J Cereb Blood Flow Metab* **33**, 1235-1241 (2013).
56. Naser, R.K.A., Hassan, A.A.K., Shabana, A.M. & Omar, N.N. Role of magnetic resonance spectroscopy in grading of primary brain tumors. *The Egyptian Journal of Radiology and Nuclear Medicine* **47**, 577-584 (2016).
57. Igarashi, H., Suzuki, Y., Huber, V.J., Ida, M. & Nakada, T. N-acetylaspartate decrease in acute stage of ischemic stroke: a perspective from experimental and clinical studies. *Magn Reson Med Sci* **14**, 13-24 (2015).
58. Moffett, J., Arun, P., Ariyannur, P. & Namboodiri, A. N-Acetylaspartate reductions in brain injury: impact on post-injury neuroenergetics, lipid synthesis, and protein acetylation. *Frontiers in Neuroenergetics* **5**(2013).
59. Yan, H.D., Ishihara, K., Serikawa, T. & Sasa, M. Activation by N-acetyl-L-aspartate of acutely dissociated hippocampal neurons in rats via metabotropic glutamate receptors. *Epilepsia* **44**, 1153-1159 (2003).
60. Alba-Arbalat, S.*, et al.* In Vivo Molecular Changes in the Retina of Patients With Multiple Sclerosis. *Investigative ophthalmology & visual science* **62**, 11-11 (2021).
61. Sanyal, S. & Bal, A.K. Comparative light and electron microscopic study of retinal histogenesis in normal and rd mutant mice. *Z. Anat. Entwicklungsgesch* **142**, 219-238 (1973).
62. Caffe, A.R.*, et al.* Mouse retina explants after long-term culture in serum free medium. *Journal of chemical neuroanatomy* **22**, 263-273 (2001).
63. Pang, Z.*, et al.* MetaboAnalyst 5.0: narrowing the gap between raw spectra and functional insights. *Nucleic acids research* (2021).